


RESEARCH

Open Access



# Absence of physiological $\text{Ca}^{2+}$ transients is an initial trigger for mitochondrial dysfunction in skeletal muscle following denervation

Cehade Karam<sup>1</sup>, Jianxun Yi<sup>1,2</sup>, Yajuan Xiao<sup>1,2</sup>, Kamal Dhakal<sup>2</sup>, Lin Zhang<sup>1,2</sup>, Xuejun Li<sup>2</sup>, Carlo Manno<sup>1</sup>, Jiejia Xu<sup>3</sup>, Kaitao Li<sup>3</sup>, Heping Cheng<sup>3</sup>, Jianjie Ma<sup>4\*</sup> and Jingsong Zhou<sup>1,2\*</sup> 

## Abstract

**Background:** Motor neurons control muscle contraction by initiating action potentials in muscle. Denervation of muscle from motor neurons leads to muscle atrophy, which is linked to mitochondrial dysfunction. It is known that denervation promotes mitochondrial reactive oxygen species (ROS) production in muscle, whereas the initial cause of mitochondrial ROS production in denervated muscle remains elusive. Since denervation isolates muscle from motor neurons and deprives it from any electric stimulation, no action potentials are initiated, and therefore, no physiological  $\text{Ca}^{2+}$  transients are generated inside denervated muscle fibers. We tested whether loss of physiological  $\text{Ca}^{2+}$  transients is an initial cause leading to mitochondrial dysfunction in denervated skeletal muscle.

**Methods:** A transgenic mouse model expressing a mitochondrial targeted biosensor (mt-cpYFP) allowed a real-time measurement of the ROS-related mitochondrial metabolic function following denervation, termed “mitoflash.” Using live cell imaging, electrophysiological, pharmacological, and biochemical studies, we examined a potential molecular mechanism that initiates ROS-related mitochondrial dysfunction following denervation.

**Results:** We found that muscle fibers showed a fourfold increase in mitoflash activity 24 h after denervation. The denervation-induced mitoflash activity was likely associated with an increased activity of mitochondrial permeability transition pore (mPTP), as the mitoflash activity was attenuated by application of cyclosporine A. Electrical stimulation rapidly reduced mitoflash activity in both sham and denervated muscle fibers. We further demonstrated that the  $\text{Ca}^{2+}$  level inside mitochondria follows the time course of the cytosolic  $\text{Ca}^{2+}$  transient and that inhibition of mitochondrial  $\text{Ca}^{2+}$  uptake by Ru360 blocks the effect of electric stimulation on mitoflash activity.

**Conclusions:** The loss of cytosolic  $\text{Ca}^{2+}$  transients due to denervation results in the downstream absence of mitochondrial  $\text{Ca}^{2+}$  uptake. Our studies suggest that this could be an initial trigger for enhanced mPTP-related mitochondrial ROS generation in skeletal muscle.

**Keywords:** E-C coupling, Calcium imaging, Calcium signaling, Calcium intracellular release, Denervation, Mitochondria

\* Correspondence: jianjie.ma@osumc.edu; jzhou@kcumb.edu

<sup>4</sup>Wexner Medical Center, The Ohio State University, 460 West 12th Avenue, Columbus, OH, USA

<sup>1</sup>Rush University School of Medicine, Chicago, IL, USA

Full list of author information is available at the end of the article



## Background

Skeletal muscle is responsible for voluntary movements of the entire body. Because it comprises around 40% of whole-body lean mass of a human, skeletal muscle is also essential for maintaining the homeostasis of the whole-body metabolism [1]. Skeletal muscle contraction is under the control of motor neurons. In some disease states, the interaction between motor neuron and skeletal muscle is lost, leading to paralysis and muscle atrophy [2]. Muscle atrophy is defined as a decrease in the muscle cell size and the imbalance between protein synthesis and degradation. The molecular mechanisms underlying protein metabolism in muscle atrophy have been extensively evaluated [3–8]. It is believed that skeletal muscle atrophy is caused by the disturbance of signaling networks, in which mitochondria may play a major role. In fact, mitochondria occupy about 10–15% of the muscle fiber volume [9]. They are not only essential for energy supply but also determine the survival or death of muscle fibers. It has been shown that denervation of skeletal muscle induces a dramatic increase in mitochondrial ROS production [10]. However, the initial cause of the mitochondrial ROS production in denervated skeletal muscle remains elusive [11].

Muscle cells use  $\text{Ca}^{2+}$  as a messenger to control events ranging from activation of contraction to cell death. Defective intracellular  $\text{Ca}^{2+}$  signaling has been linked to skeletal muscle dysfunction during aging [12, 13] and in muscular dystrophy (mdx) [14–17]. In non-muscle cells, mitochondria dynamically transport  $\text{Ca}^{2+}$  and modify its flux into the endoplasmic reticulum, nucleus, and across the plasma membrane to such an extent that they have been named “the hub of cellular  $\text{Ca}^{2+}$  signaling” [18]. There is strong evidence that mitochondria may have a similar role in skeletal muscle. We previously demonstrated that mitochondria take up  $\text{Ca}^{2+}$  during excitation-contraction (E-C) coupling following rapid calcium transients in skeletal muscle [19]. We also established that malfunction of this mechanism contributes to neuromuscular degeneration in amyotrophic lateral sclerosis [20]. Mitochondrial  $\text{Ca}^{2+}$  uptake is believed to help regulate mitochondrial metabolism and ATP synthesis, so that the energy demands of muscle contraction are met [21]. However,  $\text{Ca}^{2+}$  overload in mitochondria is also a pathological stimulus of ROS generation [22]. It has been shown that prolonged muscle denervation leads to an increased resting cytosolic free  $\text{Ca}^{2+}$  level, that in turn overloads mitochondria, stimulating ROS production [23, 24]. Following denervation, no action potential can be initiated; therefore, physiological  $\text{Ca}^{2+}$  transient is lost in the denervated muscle fibers. One essential question to ask is how mitochondria respond to the cessation of physiological  $\text{Ca}^{2+}$  transients. While published studies mainly focused on the effect of a steady

state level of intracellular  $\text{Ca}^{2+}$  on mitochondrial function, it is not known whether the dynamic change of  $\text{Ca}^{2+}$  level inside mitochondria in response to the intracellular  $\text{Ca}^{2+}$  transients is also a player in regulating mitochondrial function.

In this study, we used a transgenic mouse model carrying a mitochondrial biosensor mt-cpYFP, which produces mitoflash signal as a functional indication of ROS-related mitochondrial metabolic function [25, 26]. This model allows us to detect the early changes of ROS-related mitochondrial metabolic function in live skeletal muscle in response to the denervation process. Under voltage-clamp condition, we found that the loss of physiological  $\text{Ca}^{2+}$  transients or mitochondrial  $\text{Ca}^{2+}$  uptake could be an initial trigger for mitochondrial dysfunction with increased mitochondrial ROS production in skeletal muscle fibers following denervation.

## Methods

### Generation of transgenic mice

The plasmid (mt-cpYFP/pUCCAGGS) used to generate this transgenic line (mt-cpYFP) is the same as the one developed by Dr. Heping Cheng's Laboratory to generate the original mt-cpYFP transgenic mice [26, 27]. The genetic background for this transgenic mouse model is B6SJL from the Jackson Laboratory. The mt-cpYFP mice at the age of 2.5–3 months were used. All experiments were carried out in strict accordance with the recommendations in the Guide for the Care and Use of Laboratory Animals of the National Institutes of Health. Protocols on usage of mice were approved by the Institutional Animal Care and Use Committee of Rush University, University of Missouri at Kansas City and Kansas City University of Medicine and Bioscience.

### Muscle denervation procedure

Muscle denervation was performed by transection of the sciatic nerve. During a denervation procedure, the mouse was anesthetized with constant-flow isoflurane inhalation and a small incision was made in the mid-posterolateral area of the thigh, and the sciatic nerve was isolated. In one hind limb, the sciatic nerve was severed and a ~5 mm section was removed. The ends of the nerve were sutured to prevent nerve regrowth. For control experiments (sham), the sciatic nerve was exposed in the contralateral hind limb without being severed. The incisions in both legs were closed again with silk sutures, and the animal was euthanized after 24 h for experiments.

### Isolation of FDB fibers

The animals were euthanized by  $\text{CO}_2$  inhalation followed by cervical dislocation, and the flexor digitorum brevis (FDB) muscles were removed for imaging studies.

Individual FDB muscle fibers were isolated using a modified collagenase-digestion method described previously [19]. Briefly, FDB muscles were digested in modified Krebs solution (0  $\text{Ca}^{2+}$ ) containing 0.2% type I collagenase (Sigma), for 35 min at 37 °C. After digestion, muscles were kept in collagenase-free Krebs solution (with  $\text{Ca}^{2+}$  and 10 mM glucose) at 4 °C and used for imaging within 6 h. All experiments were conducted under the same isolation procedure and the same time window. In addition, both Sham and Denervation procedures were conducted in the same mouse, thus the paired sham and denervated FDB muscles were isolated from the same mouse for each experiment.

#### Confocal imaging of mitoflash (cpYFP) signals and image analysis

Zeiss LSM 510 live confocal microscope was used for imaging cpYFP fluorescence. Images were captured with a  $\times 40$ , 1.2 NA water immersion objective at a sampling rate of 1 s/frame. Dual excitation of mt-cpYFP was achieved by alternating excitation at 405 and 488 nm, and the emission was collected at  $>505$  nm. Experiments were performed at room temperature (23 °C). Time-lapse confocal images were analyzed using custom-developed algorithms written in Interactive Data language (IDL) [28] and ImageJ (NIH). Motion artifacts, background subtraction and photo-bleach correction were taken into account before automatic flash detection, using the built in custom-software.

#### Electric stimulation

FDB fibers isolated from denervated and sham-operated mt-cpYFP mice were bathed in Tyrode's solution. Individual fibers were electrically stimulated with a stimulation protocol described previously with some modifications [29]. Briefly, extracellular platinum wire electrodes were placed in parallel to the cell of interest. A single field stimulation of 350 ms in duration, consisting of 0.5 ms (8–12 V) pulses applied at a frequency of 40 Hz was generated. Fibers that did not visually respond to stimulation were excluded from the analysis. Mitoflash signal was monitored by collecting consecutive  $x$ - $y$  time series confocal images (100 images) immediately before electrical stimulation, 10 and 120 s after termination of the field stimulation.

#### Electroporation and gene expression in FDB muscle of adult mice

The procedure was modified from our previous study [20, 30]. The anesthetized mice were injected with 10  $\mu\text{l}$  of 2 mg/ml hyaluronidase dissolved in sterile saline at the ventral side of the hind paws through a 29-gauge needle. One hour later, 5–10  $\mu\text{g}$  of plasmid DNA of pCDNA3/mt11-YC3.6 in 10  $\mu\text{l}$  of sterile saline were

injected into the same sites. Fifteen minutes later, two electrodes (gold-plated stainless steel acupuncture needles) were placed at the starting lines of paw and toes, separated by about 9 mm. Twenty pulses of 100 V/cm with 20 ms duration were applied at 1 Hz (ECM 830 Electro Square Porator, BTX Harvard Apparatus). Seven days later, the mice were euthanized and FDB muscles were removed for functional studies.

#### Voltage clamp of FDB muscle fibers

The method was modified from our previous study [20, 31]. Muscle fibers expressing mt11-YC3.6 were patched with 0.6–1.0 M $\Omega$  pipettes filled with a cesium glutamate-based solution containing 120 mM cesium glutamate, 5 mM EGTA, 10 mM glucose, 10 mM Tris base, 5 mM ATP, 10 mM phosphocreatine, 1 mM  $\text{Mg}^{2+}$ , 100 nM  $\text{Ca}^{2+}$ , and 50  $\mu\text{M}$  M x-rhod-1. An Axopatch 200B amplifier (Axon Instruments, Foster City, CA) was used for whole-cell patch clamp. The fiber was clamped at  $-80$  mV, and changes in cytosolic  $\text{Ca}^{2+}$  transients were recorded following application of depolarizing voltages. The external solution contained 140 mM triethanolamine  $\text{CH}_3\text{SO}_3\text{H}$ , 10 mM Hepes, 1 mM  $\text{CaCl}_2$ , 3.5 mM  $\text{MgCl}_2$ , 1 mM 4-aminopyridine, 0.3 mM  $\text{LaCl}_3$ , 0.5 mM  $\text{CdCl}_2$ , 0.5  $\mu\text{M}$  tetrodotoxin, and 50  $\mu\text{M}$  *N*-benzyl-*p*-toluenesulfonamide.

#### Confocal imaging of YC3.6, x-rhod-1 and MitoSOX Red in FDB muscle fibers

We have developed a method to simultaneously record the images of YC3.6 for mitochondrial  $\text{Ca}^{2+}$  signaling and x-rhod-1 for cytosolic  $\text{Ca}^{2+}$  signaling [20]. Separate excitation and emission wavelengths were applied for simultaneous recording of x-rhod-1 and YC3.6 signals. x-rhod-1 was excited at 594 nm, and its fluorescence was collected at 600–680 nm. mt11-YC3.6 was excited at 458 nm, and its fluorescence  $f_1$  was collected at 470–520 nm and  $f_2$  at 520–580 nm. MitoSOX Red (M36008, Invitrogen) was used to evaluate mitochondrial superoxide production level. FDB muscle fibers were incubated with 0.5  $\mu\text{M}$  MitoSOX Red in our modified Krebs solution at 37 °C for 10 min. MitoSOX Red was excited at 514 nm, and its fluorescent images were collected at 570–630 nm under the Leica SP8 confocal microscope.

#### Isolation of mitochondrial fraction from skeletal muscles

Crude mitochondrial fractionations from skeletal muscle were first obtained using a method previously reported [32, 33] with some modifications. Briefly, fresh skeletal muscles were removed from the mice and placed in ice-cold phosphate-buffered saline (PBS) with 10 mM EDTA. The muscles were suspended in 10 ml/gram weight ice-cold homogenization buffer (100 mM sucrose, 10 mM EDTA, 100 mM Tris-HCl, 46 mM KCl,

pH 7.4 with 5 mg/ml BSA and proteinase inhibitor (Thermo Fisher), minced into small pieces and homogenized on ice. The homogenate was centrifuged at 800g 4 °C for 10 min. The supernatant was transferred to a new centrifuge tube and centrifuged at 10,000g 4 °C for 10 min. The resulting pellets were the crude mitochondrial fraction. The supernatant was centrifuged at 100,000g 4 °C for 60 min. The final supernatant was the pure cytosolic fraction.

The crude mitochondrial fractions were suspended in 1.5 ml 25% nycodenz buffer, layered onto 1.25 ml 30% nycodenz buffer, and overlaid with 1.25 ml 23% nycodenz buffer containing 5 mM Tris, 3 mM KCl, 0.3 mM EDTA, and pH7.5. The samples were centrifuged at 52,000 for 90 min at 4 °C in a swinging bucket rotor (BECKMAN, SW60 Ti). The mitochondrial fraction was collected from the 25%/30% interface and resuspended in equal volume of homogenization buffer and centrifuged at 10,000g at 4 °C for 10 min. This step was repeated for three times. The pure mitochondria fraction in the final pellet was used for the immunoblot assay.

#### Immunoblot assay

Protein concentrations were determined by BCA protein assay (Thermo Scientific). Equal mass protein samples (10  $\mu$ g) were subjected to 10% SDS-polyacrylamide gel electrophoresis, transferred to PVDF membrane (MILIPORE), and immunoblotted with primary antibodies. The antibodies used were anti-Cyclophilin F (Abcam, ab110324), 1:1000 dilution; anti-COX-IV (Cell Signaling, 4844S), 1:5000 dilution and anti-GAPDH (Cell signaling, 5174S), 1:10000 dilution. Results were visualized with ECL reagents (Thermo Scientific). Densitometry evaluation was conducted using ImageJ software (NIH, Bethesda, MD).

#### Statistics

Statistical comparisons were done using students *t* test for single mean or ANOVA test for multiple means when appropriate. All graphs were plotted in Sigmaplot (Systat Software Inc.) and results were expressed as mean  $\pm$  S.E., and  $p < 0.05$  was considered significantly different.

## Results

### Denervation leads to drastic increase of mitoflash signal in skeletal muscle fibers

Based on the biochemical study of Muller et al. [10], it has been shown that the ROS production increases 30-fold in skeletal muscle after 7 days of denervation. The initial response of mitochondria to denervation in skeletal muscle has not been studied. The mt-cpYFP transgenic mouse model provides a useful tool to examine the dynamic changes of mitochondrial ROS production in the form of mitoflash signaling in live skeletal

muscle cells [25, 26]. While there is ongoing debate regarding the mt-cpYFP sensitivity to ROS and pH [34], resolution of the spatial and temporal aspects of mitoflash signals has been widely used to explore the changes in the metabolic function of mitochondria under physiological and pathological conditions [35].

The mt-cpYFP transgenic mice were generated in our laboratory. The mitochondrial targeting of mt-cpYFP is demonstrated in the Additional file 1: Figure S1. The FDB muscle fibers derived from the mt-cpYFP mice were isolated for live cell imaging to record the mitoflash activity. A standard protocol was established to record the mitoflash events in FDB muscle fibers, in which 100 images were taken continuously at a speed of 1 image/s. The mitoflash signal was analyzed using the established software, FlashSniper [28], to obtain parameters of the mitoflash signal including full area at half maximum (FAHM), full duration at half maximum (FDHM), and the amplitude of the signal ( $dF/F_0$ ). In addition, the fiber area giving mitoflash signal during the 100-sequential-imaging time period was summed as Total Flash Area. The ratio of Total Flash Area over the whole fiber area named Total Flash Area/Fiber Area was then calculated. Total Flash Area/Fiber area during this 100-sequential-image recording time period provides quantification of the number of mitochondria in a single muscle fiber that are involved in generating mitoflash events, as well as the frequency of the mitoflash events.

To determine the dynamic response of mitochondrial metabolic function of skeletal muscle to denervation, the sciatic nerve transection procedure was conducted at one hind limb of the mt-cpYFP mouse. A sham procedure without sciatic nerve transection was conducted on the contralateral hind limb of the same mt-YFP mouse as the control. To catch the early response of mitochondria to denervation, FDB muscle fibers were isolated for evaluating mitoflash activity 24 h after the procedure. Compared with the sham operation, the denervation resulted in a dramatic increase of mitoflash activity in muscle fibers as shown in the movies (Additional files 2 and 3: Movies 1 and 2) and representative images of a denervated muscle fiber in Fig. 1b1–3. In sham cells, mitoflash events were limited to localized areas of the muscle fiber represented by small patches (Fig. 1a1–3). Upon denervation, there was a significant increase in the fiber area in which mitochondria showed mitoflash signal (Fig. 1b2–3) as quantified by the Total Flash Area/Fiber Area plotted in Fig. 1d (Sham;  $1.65 \pm 0.36$ ,  $n = 64$  cells vs Den;  $7.77 \pm 1.87$ ,  $n = 59$  cells;  $p < 0.001$ ). This correlated well with the increase in FAHM (Fig. 1e) of the mitoflash signal (Sham;  $20.36 \pm 3.6$ ,  $n = 64$  muscle fibers vs Den;  $83.43 \pm 19.14$  in  $\mu\text{m}^2$ ,  $n = 59$  muscle fibers;  $p < 0.001$ ). Despite the dramatic increase in FAHM of the mitoflash signal in denervated muscle fibers, there

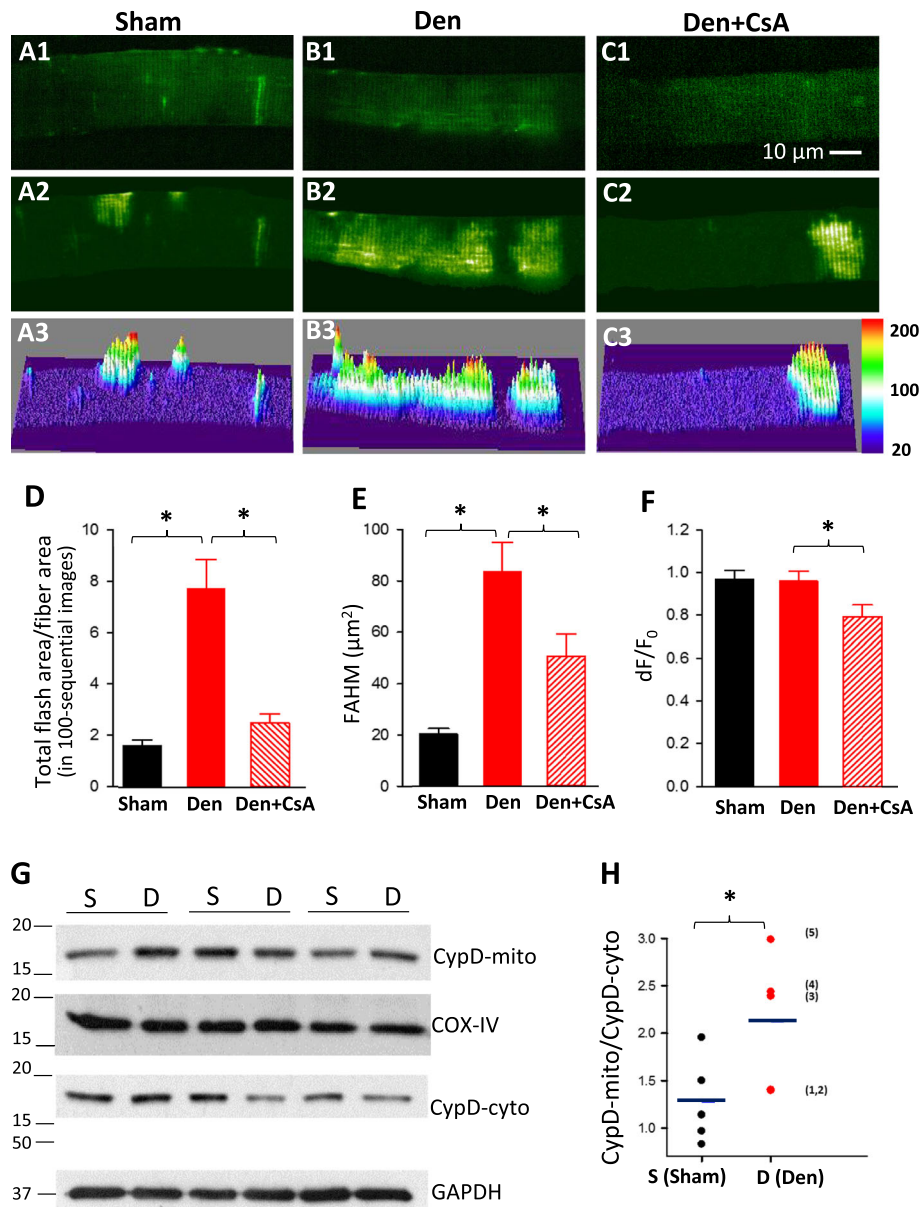


**Fig. 1** Denervated muscle fibers show an enhanced mitoflash activity, and CypD is involved in this activity. The representative confocal images of muscle fibers isolated from the FDB muscles with sham (**a1–3**), denervation (Den) (**b1–3**), and denervation + CsA treatment (Den + CsA) (**c1–3**). Panels **a1**, **b1**, and **c1** show the initial fluorescence images at  $t = 0$  s. Panels **a2**, **b2**, and **c2** show the peak intensity map of all mitoflashes detected in 100 recorded images. Panels **a3**, **b3**, and **c3** are the 3D surface plots of (**a2**, **b2**, and **c2**). The quantification analysis of the mitoflashes for three conditions are illustrated in **d** Total Flash Area/Fiber Area (in 100 sequential images), **e** FAHM, and **f** the amplitude ( $dF/F_0$ ) of the mitoflashes. Note that live skeletal muscle fibers respond to the 24-h denervation with dramatically increases of the mitoflash signal in mitochondria, while the CsA treatment restored the Total Flash Area/Fiber Area close to the normal level and significantly reduced the FAHM and signal amplitude ( $n = 57–64$ ,  $*p < 0.05$ ). **g** Immunoblot assay of CypD expression level in both mitochondria (CypD-mito) and cytosol (CypD-cyto) of the skeletal muscle with and without 24-h denervation. **h** The ratio of CypD in mitochondria over the CypD in cytosol (CypD-mito/CypD-cyto) was quantified. The annotated numbers in parentheses indicate the individual immunoblot assay experiments for denervated skeletal muscle. Note that the 24-h denervation promoted the translocation of CypD from cytosol to mitochondria ( $n = 5$ ,  $*p < 0.05$ )

were no significant changes in other parameters of the mitoflash signal including the amplitude  $dF/F_0$  ( $0.97 \pm 0.07$ ,  $n = 64$  muscle fibers and  $0.96 \pm 0.09$ ,  $n = 59$  muscle fibers;  $p = 0.875$ ) and the FDHM ( $14.47 \pm 2.43$ ,  $n = 58$  muscle fibers and  $17.84 \pm 2.04$ ,  $n = 59$  muscle fibers;

$p = 0.08$ ) compared with the sham muscle fibers. These data indicate that in response to denervation, the number of mitochondria producing ROS is increased in the skeletal muscle, while the intensity and the duration of the ROS production of individual mitochondrion remain unchanged.

### Cyclosporine A attenuates the increase of mitoflash activity caused by denervation

It has been shown that mitoflash signal is associated with transient opening of the mitochondrial permeability transition pore (mPTP) in both cardiac and skeletal muscle [26, 27]. However, two published studies reported that CsA did not affect the mitoflash signal in normal skeletal muscle [36, 37], suggesting the possibility that the mitoflash signal is not related to Cyclophilin D (CypD) under physiological conditions. Here, we tested whether mitoflash activity became CypD-dependent upon denervation. We examined whether altered mPTP opening was associated with the generation of massive mitoflash signal in denervated skeletal muscle and whether inhibition of CypD-dependent pore opening could restore mitoflash activity to the normal level in denervated muscles. Muscle fibers isolated from denervated skeletal muscle were treated with 1  $\mu$ M Cyclosporine A (CsA) for 30 min prior to imaging. Additional file 4 (movie 3) and Fig. 1c1–3 show representative images of denervated muscle treated with CsA. The application of CsA significantly decreased the flashing area (Total Flash Area/Fiber Area) in denervated muscle fibers (Fig. 1d; Den  $7.77 \pm 1.87$ ,  $n = 59$  muscle fibers vs Den + CsA  $2.50 \pm 0.63$ ,  $n = 57$  muscle fibers;  $p < 0.001$ ). In line with those results, the size of mitoflash signal (FAHM) was also significantly reduced (Fig. 1e; Den  $83.43 \pm 19.14$ ,  $n = 59$  muscle fibers vs Den + CsA  $50.45 \pm 14.96$ ,  $n = 57$  muscle fibers,  $p = 0.023$ ). Interestingly, the flash amplitude  $dF/F_0$  was significantly reduced after the CsA treatment (Fig. 1f; Den  $0.96 \pm 0.09$ ,  $n = 59$  muscle fibers, Den + CsA  $0.79 \pm 0.10$ ,  $n = 57$  muscle fibers;  $p = 0.02$ ). No change in FDHM was observed among the groups. These results indicate that the opening of mPTP plays an important role in the mitochondrial ROS production in the denervated skeletal muscle cells.

Because CypD plays a critical role in controlling mPTP activity, we conducted immunoblot analysis to evaluate the protein expression level of CypD in both mitochondria and cytosol of the skeletal muscle following 24 h of denervation. We first confirmed the purity of mitochondrial and cytosol fractionation by using specific markers for mitochondria (COX-IV) and cytosol (GAPDH). As demonstrated in Additional file 5: Figure S2, the pure mitochondria fractions do not contain GAPDH, while the cytosol portion does not contain COX-IV, indicating no cross-contamination between the mitochondrial and cytosol fractionations. The level of CypD in mitochondria (CypD-mito) and cytosol (CypD-cyto) was quantified by normalization to the mitochondrial and cytosol specific markers, respectively, prior to the calculation of the CypD-mito to CypD-cyto ratio. We found that the ratio of CypD level in mitochondria to the CypD level in cytosol (CypD-mito/CypD-cyto) was significantly increased in the denervated muscle compared with the sham-treated

muscle (sham  $1.28 \pm 0.20$  vs Den  $2.12 \pm 0.31$ ,  $n = 5$ ,  $p < 0.05$ ) (Fig. 1g and h). The data provide additional support that the denervation-induced mitoflash signal is likely related to CypD-dependent pore opening of the mPTP.

### Electric stimulation reduces mitoflash activity in both sham and denervated muscle fibers

The sciatic nerve transection isolates the muscle from the central nervous system and deprives it from any electric stimulation, which results in the absence of action potentials and physiological  $Ca^{2+}$  transients in the denervated muscle fibers. We hypothesize that the loss of physiological  $Ca^{2+}$  transients may contribute to the elevated mitochondrial ROS production. Thus, we tested whether restoration of physiological  $Ca^{2+}$  transient could eliminate the enhanced mitochondrial ROS product induced by denervation. We applied a brief field electric stimulation (350 ms) on isolated muscle fibers to initiate  $Ca^{2+}$  transients and evaluated the mitoflash activity shortly after the electric stimulation. Fibers that did not visually respond to stimulation were excluded from the study. Additional files 6 and 7 (movie 4 and 5) and Fig. 2 show representative images of muscle fibers isolated from the denervated (Fig. 2a1–9, Additional file 7: Movie 5) and sham muscles (Fig. 2b1–9, Additional file 6: Movie 4), before, 10 and 120 s after the electric stimulation. Quantitation of the mitoflash area (Total Flash Area/Fiber Area) of the muscle fiber (Fig. 2c) shows a persistent and significant decrease at 10 and 120 s respectively in both sham (sham  $1.62 \pm 0.46$ ,  $0.1 \pm 0.09$ ,  $0.16 \pm 0.22$ ,  $n = 17–24$ ;  $p < 0.001$ ) and denervated ( $11.53 \pm 2.87$ ,  $3.74 \pm 2.38$ ,  $1.89 \pm 1.87$ ,  $n = 18–20$ ;  $p < 0.001$ ) muscle fibers. In addition, the flashing area in denervated fibers at 120 s after stimulation was reduced to a level similar to that observed in sham fibers before the stimulation (sham before stimulation,  $1.62 \pm 0.46$ ,  $n = 24$ ; Den + Stim at 120 s,  $1.89 \pm 1.87$ ,  $n = 20$  cells;  $p = 0.792$ ). The changes were also observed in FAHM (Fig. 2d) in both sham ( $23.38 \pm 9.33$ ,  $2.72 \pm 1.92$ ,  $2.87 \pm 3.45$ ,  $n = 19–24$ ;  $p < 0.001$ ) and denervated ( $131.73 \pm 65.79$ ,  $27.13 \pm 13.26$ ,  $27.96 \pm 29.62$ ,  $n = 20$  cells;  $p < 0.05$ ) cells. Furthermore, the stimulation had a significant effect on the mitoflash amplitude  $dF/F_0$  (Fig. 2e) that was reduced at 10 and 120 s, respectively, in sham ( $0.82 \pm 0.09$ ,  $0.12 \pm 0.09$ ,  $0.04 \pm 0.05$ ,  $n = 19–24$ ;  $p < 0.001$ ) and denervation ( $0.86 \pm 0.12$ ,  $0.22 \pm 0.12$ ,  $0.09 \pm 0.07$ ,  $n = 20$ ;  $p < 0.001$ ). These results are in line with the effects of CsA on the mitoflash amplitude (Fig. 1f). However, compared with the effect of CsA, the data indicate that the electric stimulation has a more potent effect on reducing the mitoflash activity.

Since the mitoflash activity in the denervated muscle fibers was dramatically reduced by an electric field stimulation, we hypothesize that  $Ca^{2+}$  uptake into mitochondria

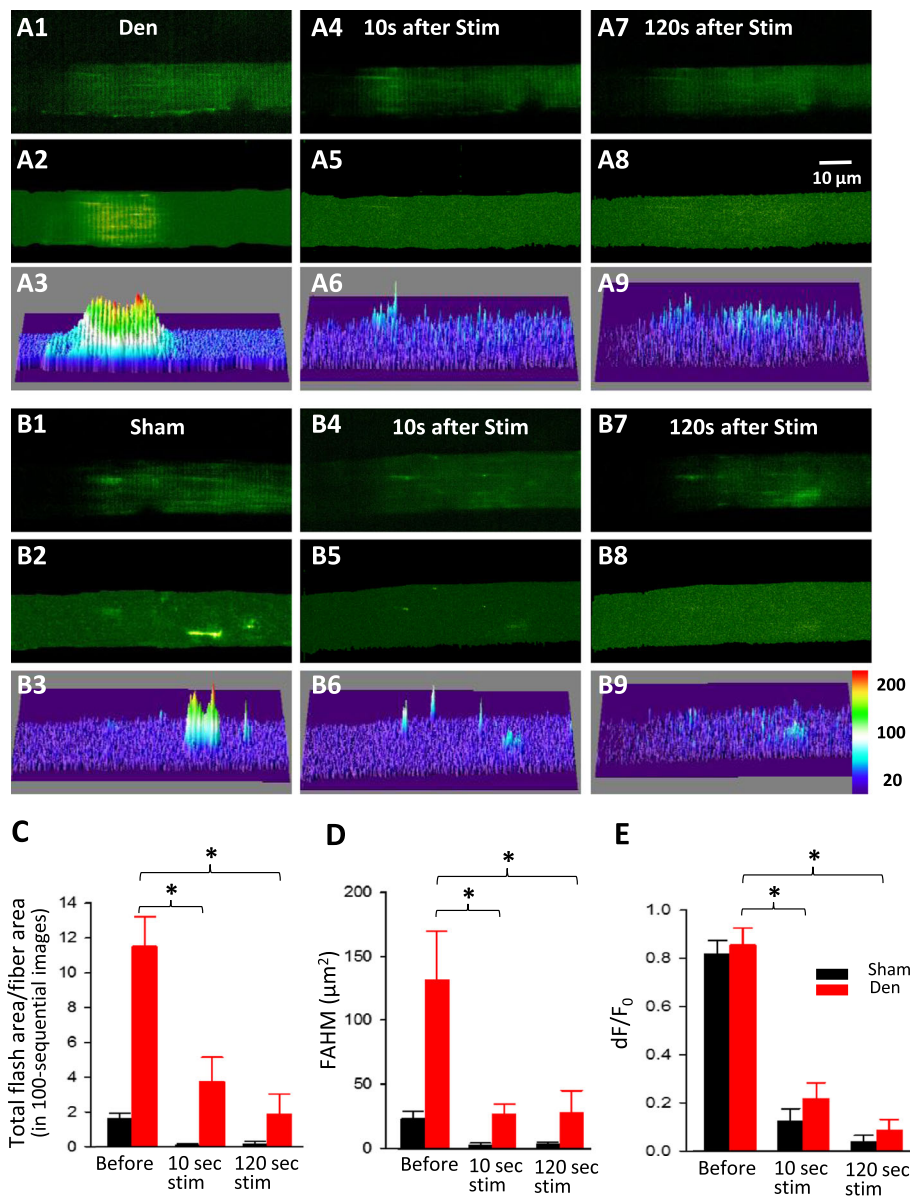


**Fig. 2** Electric stimulation eliminated the effects of denervation on the mitoflash activity. The representative confocal images of muscle fibers isolated from the denervated FDB muscle before field stimulation (Den) (a1–3), 10 s after the field stimulation (a4–6), and 120 s after the field stimulation (a7–9). Panels a1, a4, and a7 show the initial fluorescence images at  $t = 0$  s. Panels a2, a5, and a8 show the peak intensity map of all mitoflashes detected in 100 recorded images. Panels a3, a6, and a9 are the 3D surface plots of (a2, a5, and a8). The representative confocal images of muscle fibers isolated from the sham FDB muscle before field stimulation (sham) (b1–3), 10 s after the field stimulation (b4–6), and 120 s after the field stimulation (b7–9). Panels b1, b4, and b7 show the initial fluorescence images at  $t = 0$  s. Panels b2, b5, and b8 show the peak intensity map of all mitoflashes detected in 100 recorded images. Panels b3, b6, and b9 are the 3D surface plots of (b2, b5, and b8). The quantification of the mitoflashes are illustrated in **c** Total Flash Area/Fiber Area, **d** FAHM, and **e** the signal amplitude

may have a potential role in control of mitoflash activity during a physiological  $\text{Ca}^{2+}$  release transient. Thus, we tested whether pharmacological inhibition of the mitochondrial  $\text{Ca}^{2+}$  uptake by Ru360, an inhibitor of mitochondrial uniporter [19, 38] could block the effect of the field stimulation on the denervated muscle fibers. The control (sham) and denervated FDB muscle fibers were first incubated with 10  $\mu\text{M}$  Ru360 for 30 min before

receiving the field stimulation. As shown in Fig. 3, in the presence of Ru360, the field stimulation had no significant effect on the mitoflash activity of muscle fibers. The Total Flash Area/Fiber Area of denervated fibers in the presence of Ru360 before and after the stimulation are  $7.12 \pm 2.31$  and  $4.91 \pm 3.24$  ( $n = 5$ ,  $p > 0.05$ ). The (Total Flash Area/Fiber Area) of sham in the presence of Ru360 before and after stimulation is  $2.22 \pm 0.73$  and  $1.99 \pm 0.99$

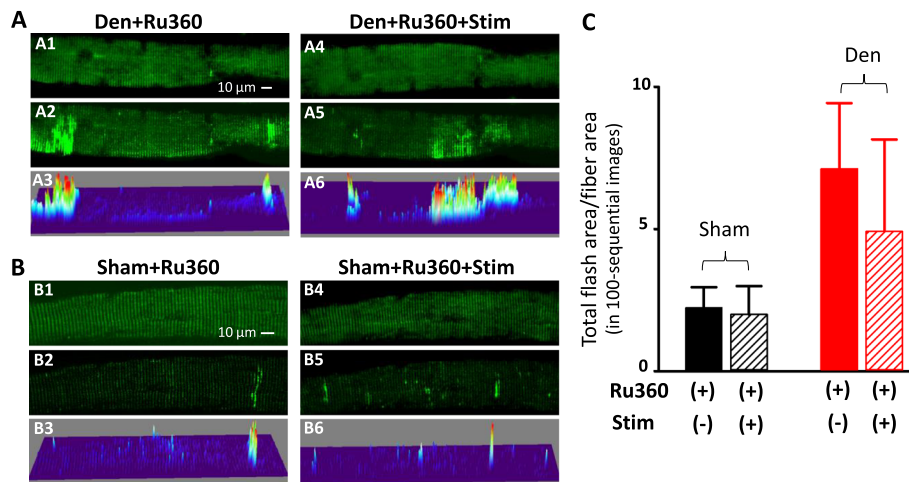


**Fig. 3** Ru360 eliminated the effect of field stimulation on mitoflash activity. The representative confocal images of muscle fibers isolated from the denervated FDB muscle fibers before field stimulation (Den **a1–3**), and 120 s after the field stimulation (**a4–6**) in the presence of 10  $\mu$ M Ru360. Panels **a1** and **a4** show the initial fluorescence images at  $t = 0$  s. Panels **a2** and **a5** show the peak intensity map of all mitoflashes detected in 100 recorded images. Panels **a3** and **a6** are the 3D surface plots of (**a2** and **a5**). The representative confocal images of muscle fibers isolated from the sham FDB muscle before the field stimulation (sham) (**b1–3**), 120 s after the field stimulation (**b4–6**). Panels **b1** and **b4** show the initial fluorescence images at  $t = 0$  s. Panels **b2** and **b5** show the peak intensity map of all mitoflashes detected in 100 recorded images. Panels **b3** and **b6** are the 3D surface plots of (**b2** and **b5**) in the presence of 10  $\mu$ M Ru360. The quantification of the Total Flash Area/Fiber Area of the mitoflashes is summarized in (c). Note that in the presence of Ru360, there are no significant changes in mitoflash activity before and after the field stimulation ( $n = 5$ ,  $p > 0.05$ )

( $n = 5$ ,  $p > 0.05$ ). Similarly, FAHM of sham fibers before and after stimulation are  $14.29 \pm 3.96$  and  $9.26 \pm 5.30$  ( $n = 5$ ,  $p > 0.05$ ) and that of denervated fiber are  $56.75 \pm 15.89$  and  $61.20 \pm 20.80$ , respectively, ( $n = 5$ ,  $p > 0.05$ ). The mitoflash intensity ( $dF/F_0$ ) before and after the field stimulation in the presence of Ru360 for sham fibers are  $1.71 \pm 0.13$  and  $1.71 \pm 0.08$  ( $n = 5$ ,  $p > 0.05$ ) and for denervated fibers are  $1.71 \pm 0.14$  and  $1.66 \pm 0.09$  ( $n = 5$ ,  $p > 0.05$ ). In addition, the application of Ru360 did not lead to significant changes in mitoflash activity in both sham and denervated muscle fibers before the electric stimulation (see Total Flash Area/Fiber Area in Figs. 1d, 2c, and 3c). These data suggest that the transient mitochondrial  $Ca^{2+}$  uptake is likely responsible for suppressing the mitoflash activity during a physiological  $Ca^{2+}$  release transient.

#### Electrical stimulation and CsA treatment reduces the recurrence of mitoflash events in denervated skeletal muscle

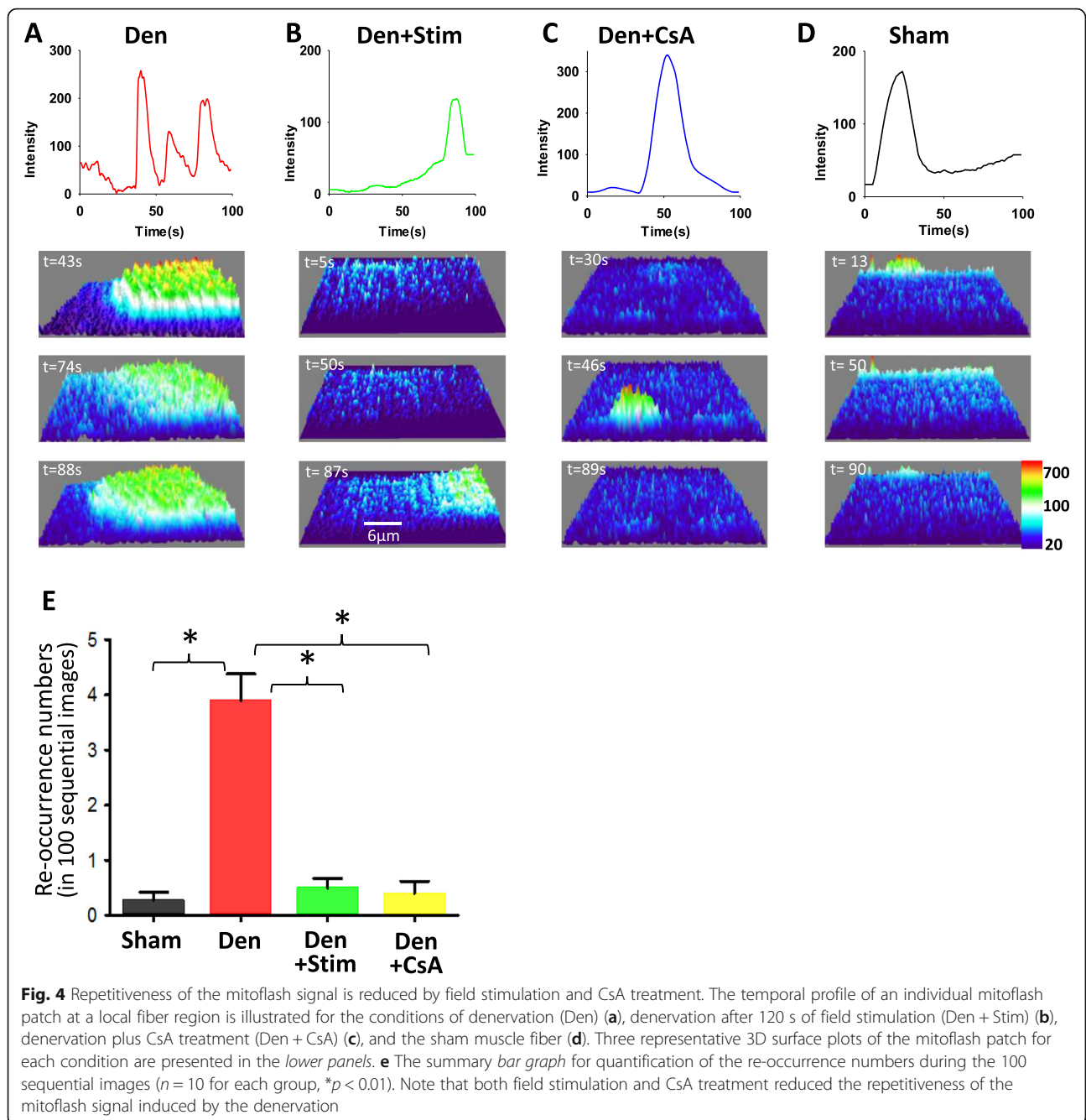
Two major changes of skeletal muscle fibers following denervation are the larger size of the mitoflash signal (FHAM) and the Flash Area/Fiber Area during the 100 s recording period (one image/s). The four- to fivefold increase in the Flash Area/Fiber Area in the denervated muscle fibers not only indicates more mitochondria being activated to generate mitoflash events but also suggests an increased frequency of mitochondria to produce

mitoflash events during the 100 s recording time period. By focusing on a region of interest (ROI) when examining individual images recorded during the 100 s period, we found that mitochondria in the denervated muscle fibers displayed more recurrence of the mitoflash activity during the 100 s recording period. As shown in Fig. 4a, a denervated muscle fiber displayed mitoflash events three times during the 100 s recording period at one local fiber area (ROI), while in a sham muscle fiber, the mitoflash signal appeared only once during the 100 s recording period (Fig. 4d). The results further suggest that denervation indeed results in repetitive opening of the mPTP. Remarkably, both field stimulation and CsA treatment decreased the reoccurrence of the mitoflash signal induced by the denervation as shown in Fig. 4b–c. The reoccurrence numbers of mitoflash events during 100 sequential images for each experimental group are summarized in Fig. 4e.

#### Mitochondria $Ca^{2+}$ transient follows the physiological intracellular $Ca^{2+}$ transient

The field electric stimulation of FDB fibers mimics the nerve stimulation by inducing action potentials in muscle fibers that lead to physiological  $Ca^{2+}$  release from the sarcoplasmic reticulum (SR) and dynamic changes of intracellular  $Ca^{2+}$  level named  $Ca^{2+}$  transients. We ask whether the free  $Ca^{2+}$  level inside mitochondria follows the intracellular  $Ca^{2+}$  transient and whether it may be associated with mitochondrial ROS production. We have previously established





a way to quantify mitochondrial  $Ca^{2+}$  uptake in skeletal muscle fibers using mitochondria-targeted  $Ca^{2+}$  biosensor mt-YC3.6 under the voltage-clamp condition and demonstrated that the level of mitochondria  $Ca^{2+}$  synchronizes with the cytosolic  $Ca^{2+}$  transient during a brief membrane depolarization with 10 ms duration [20]. Since the duration of the field stimulation applied to reduce the denervation-induced mitoflash signal was 350 ms, we examined whether  $Ca^{2+}$  transients in mitochondria also follows the time course of the cytosolic  $Ca^{2+}$  transients during a prolonged membrane depolarization using FDB muscle transfected

with mt-YC3.6. Ideally, if we could measure the mitochondrial  $Ca^{2+}$  level in cpYFP muscle fibers, the fluorescence spectra of cpYFP and mt-YC3.6 overlap each other. Thus, we have quantified mitochondrial  $Ca^{2+}$  uptake following a voltage-induced  $Ca^{2+}$  release in mt-YC3.6 muscle fibers without cpYFP expression. As shown in Fig. 5a, the muscle fiber transfected with mt-YC3.6 has mitochondria-targeted pattern. The YC3.6 protein functions as a ratiometric  $Ca^{2+}$  probe [39] because its fluorescence changes in opposite directions at two wavelengths ( $f_1$  and  $f_2$ ) as shown in Fig. 5c in response to  $Ca^{2+}$  release from the SR (Fig. 5c,  $f_3$ ).  $f_2$  vs  $f_1$

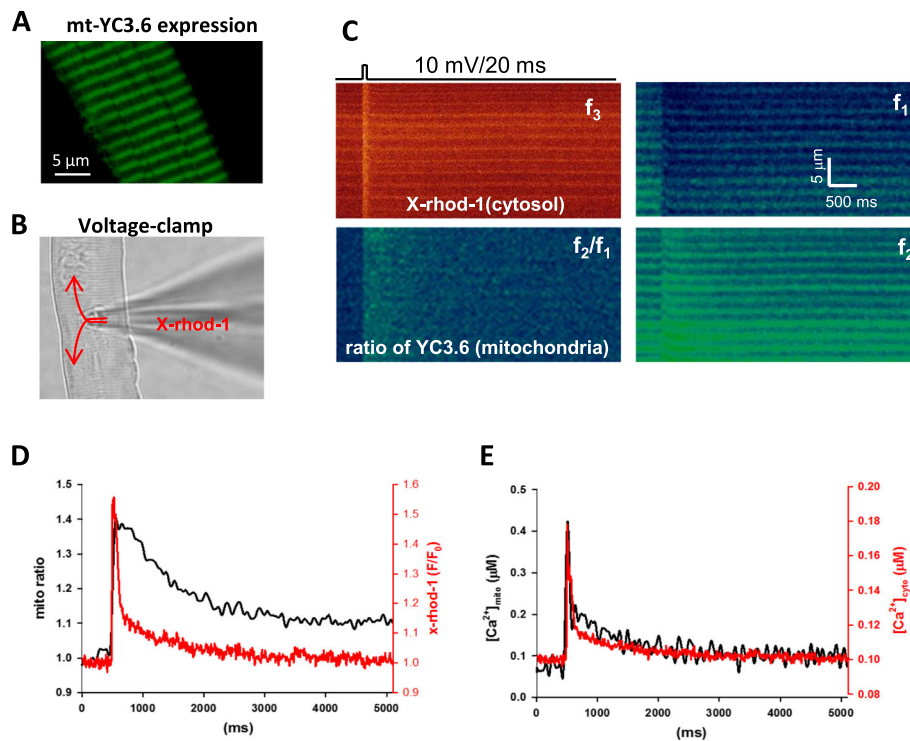


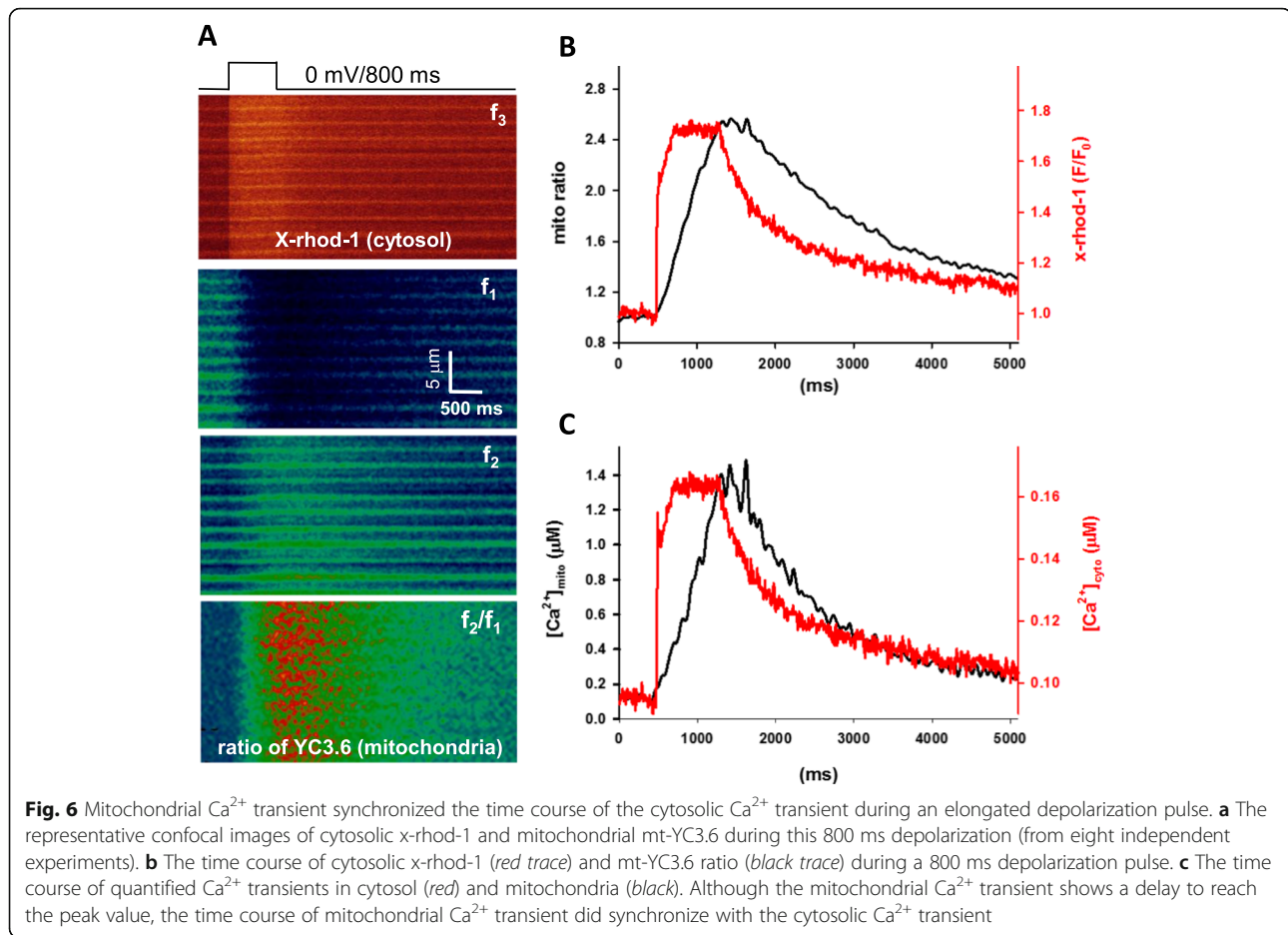
**Fig. 5** Simultaneous recording of cytosolic and mitochondrial  $\text{Ca}^{2+}$  transients. **a** A representative confocal image of FDB fiber expressing mt-YC3.6. Note the mitochondrial expression pattern of mt-YC3.6. **b** A representative image of an FDB fiber that is voltage-clamped through a glass pipette (from eight independent experiments). x-rhod-1 is delivered into the cytosol of the fiber through the pipette for recording of cytosolic  $\text{Ca}^{2+}$  transients. **c** Simultaneous recording of the dynamic changes of  $\text{Ca}^{2+}$  in both cytosol and mitochondria. Panels  $f_3$  and  $f_2$  are the fluorescence changes of mt-YC3.6 at different emission wavelengths. Panel  $f_2/f_1$  is the ratio of mt-YC3.6 images. **d** The time course of cytosolic x-rhod-1 (red trace) and mitochondrial mt-YC3.6 ratio (black trace) following a brief depolarization pulse (20 ms). **e** The time course of quantified  $\text{Ca}^{2+}$  transients in cytosol (red) and mitochondria (black). Note the similar time courses of cytosolic and mitochondrial  $\text{Ca}^{2+}$  transients

wavelengths represent the  $\text{Ca}^{2+}$  bound vs unbound states, respectively. The ratio of  $f_2/f_1$  (mito ratio) indicates an increase of  $[\text{Ca}^{2+}]$  inside mitochondria upon voltage-induced  $\text{Ca}^{2+}$  release (Fig. 5d, black trace). The dynamic change of free  $\text{Ca}^{2+}$  level in mitochondria (mitochondrial  $\text{Ca}^{2+}$  transient) (Fig. 5e, black trace) was calculated using the method established in our previous work [20].

The patch pipette solution contained x-rhod-1, a fast cytosolic  $\text{Ca}^{2+}$  indicator with excitation and emission spectra distinct from those of mt11-YC3.6. The x-rhod-1 delivered into the cytosol of the muscle fiber (Fig. 5b) allows the recording of  $\text{Ca}^{2+}$  transients in the cytosol simultaneously with mitochondrial signal recording of mt-YC3.6 (Fig. 5c,  $f_3$ ). The change in fluorescence intensity  $F/F_0(t)$  of x-rhod-1 (Fig. 5d, red trace) was used to derive the intracellular  $\text{Ca}^{2+}$  transient, and the changes in mito ratio  $f_3$  ( $f_2/f_1$ ) (Fig. 5d, black trace) was used to derive the mitochondrial  $\text{Ca}^{2+}$  uptake using the same method described in our previous work [20] (Fig. 5e). Figure 5e demonstrates that the dynamic change of  $\text{Ca}^{2+}$  level in mitochondria (Fig. 5e, black trace) indeed follows the dynamic change of  $\text{Ca}^{2+}$  level in the cytosol

(Fig. 5e, red trace). Following a short (20 ms) depolarization stimulation, the time courses of  $\text{Ca}^{2+}$  transients are very similar in both mitochondria and cytosol.

We next examined whether mitochondrial  $\text{Ca}^{2+}$  transients synchronized with the cytosolic  $\text{Ca}^{2+}$  transients during a longer depolarization pulse of 800 ms. As demonstrated in Fig. 6, the FDB muscle fiber expressing mt-YC3.6 was stimulated with a depolarization pulse of 800 ms. This elongated stimulation induced an elongated  $\text{Ca}^{2+}$  release signal in the cytosol (Fig. 6a, the panel  $f_3$  and Fig. 6b, the red trace of x-rhod-1). The simultaneously recorded mt-YC3.6 signals (Fig. 6a, panels  $f_1$  and  $f_2$ ) provided a recording of mitochondrial  $\text{Ca}^{2+}$  uptake represented by the ratio of  $f_2/f_1$  (Fig. 6a, panel  $f_2/f_1$ ). Both quantified cytosolic and mitochondrial  $\text{Ca}^{2+}$  transients induced by the elongated depolarization pulse are depicted in Fig. 6c (the red trace for cytosolic  $[\text{Ca}^{2+}]$  and the black trace for mitochondrial  $[\text{Ca}^{2+}]$ ). During the elongated depolarization, there was a delay for mitochondrial  $\text{Ca}^{2+}$  transient to reach its peak value. However, the mitochondrial  $\text{Ca}^{2+}$  transient was synchronized with the cytosolic  $\text{Ca}^{2+}$  transient. The data



demonstrates that the  $\text{Ca}^{2+}$  level in mitochondria indeed follows the dynamic changes of the  $\text{Ca}^{2+}$  level in cytosol. In the case of denervation, no action potential is initiated by the motor neurons, thus there are no cytosolic  $\text{Ca}^{2+}$  transients, and therefore, no mitochondrial  $\text{Ca}^{2+}$  transients either. It is possible that dynamic alterations of mitochondrial  $\text{Ca}^{2+}$  transients may be essential to maintain the normal mitochondrial function in skeletal muscle. The absence of dynamic alterations of mitochondrial  $\text{Ca}^{2+}$  transients may be associated with the enhanced mitoflash activity, which is linked to the enhanced mitochondrial ROS generation following the denervation.

#### Using MitoSOX Red to evaluate the role of intracellular $\text{Ca}^{2+}$ transients on mitochondrial ROS production

Because of the ongoing debate of the mt-cpYFP sensitivity on ROS and pH [34], we used MitoSOX Red, a commercially available dye to further evaluate the response of denervated muscle fibers to the electric field stimulation. MitoSOX Red is a fluorogenic dye for highly selective detection of superoxide and is rapidly and selectively targeted to mitochondria. Once in mitochondria, MitoSOX Red is oxidized by superoxide and exhibits red

fluorescence (M36008, Invitrogen). This reaction is not reversible and MitoSOX Red is not able to follow the dynamic changes of the mitochondrial superoxide level before and after the field stimulation in a single muscle fiber. However, its relative fluorescent intensity can be used to compare the basal mitochondrial superoxide production level among different muscle fibers when experimental conditions, such as the dye loading and the confocal microscope setting, are kept the same. We first loaded the FDB muscle fibers derived from the sham and the denervated legs of the same mouse with MitoSOX Red. As demonstrated in Figs. 7a1–2 and 6b, the fluorescent intensity of MitoSOX Red is significantly higher in the denervated muscle fibers (sham  $6.29 \pm 2.21$  vs denervation  $13.87 \pm 3.80$ ,  $n = 5, 11$ ,  $p < 0.001$ ). In the second set of experiments, we tested whether the electric field stimulation could reduce the fluorescent intensity of MitoSOX Red in the denervated FDB muscle fibers. The denervated FDB muscle fibers were first set to a glass bottom culture dish. A few denervated muscle fibers were selected to receive the electric field stimulation. Immediately after the electric field stimulation, the MitoSOX Red was added into the dish following the

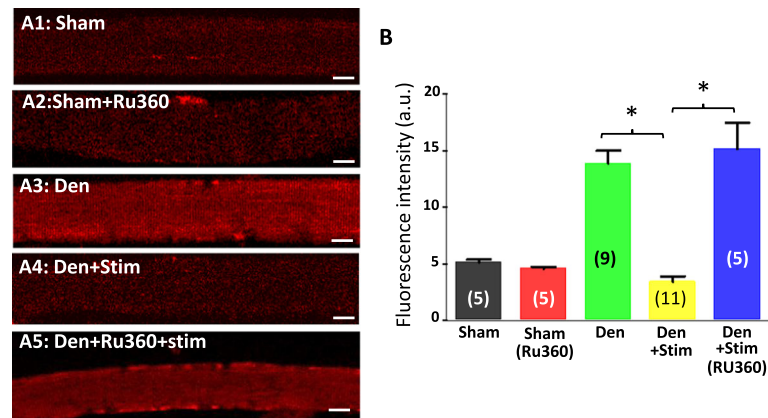


**Fig. 7** The effect of denervation on mitochondrial ROS production evaluated by MitoSOX Red. Muscle fibers were loaded with the mitochondrial superoxide indicator, MitoSOX Red. Panels **a1** and **a2** are the representative images of sham muscle fibers in the absence and presence of 10  $\mu\text{M}$  Ru360, which inhibits the mitochondrial  $\text{Ca}^{2+}$  uptake through the mitochondrial uniporter. Note that Ru360 has no significant effect on mitochondrial superoxide production level. Panel **a3** is the representative image of denervated muscle fibers. Panels **a4** and **a5** are the representative images of denervated muscle fibers received the electric field stimulation in the absence and presence of 10  $\mu\text{M}$  Ru360. **b** Quantification of the relative MitoSOX Red fluorescence intensity at those different experimental conditions. Note that the denervated muscle fibers show enhanced MitoSOX Red fluorescence intensity (**a3**), while the electric field stimulation reduced the denervation-induced increase in MitoSOX Red intensity (**a4**), and Ru360 significantly blocked the effect of the field stimulation on the denervated muscle fiber (**a5**) ( $n = 5-11$ ,  $*p < 0.05$ ). Bar, 20  $\mu\text{m}$

same dye loading procedure. The MitoSOX Red intensity of the denervated muscle fibers was then evaluated. As shown in Figs. 7a3 and 6b, the denervated muscle fibers received the field stimulation showed significantly lower MitoSOX Red intensity ( $3.41 \pm 1.41$ ,  $n = 9$ ,  $p < 0.001$  compared to the fibers without field stimulation). This set of data suggest that mitochondria in denervated skeletal muscle indeed response to the physiological intracellular  $\text{Ca}^{2+}$  transients with reduced superoxide production.

Since our voltage-clamp data demonstrated that  $\text{Ca}^{2+}$  level in mitochondria followed the dynamic changes of cytosolic  $\text{Ca}^{2+}$  level and Ru360 blocked the effect of electric stimulation on mitoflash activity (Fig. 3), we hypothesize that mitochondrial  $\text{Ca}^{2+}$  uptake may affect the superoxide production during a physiological  $\text{Ca}^{2+}$  release transient. As in Fig. 3, we further tested whether pharmacological inhibition of the mitochondrial  $\text{Ca}^{2+}$  uptake by Ru360 could block the effect of the field stimulation on the denervated muscle fibers labeled with MitoSOX Red. The denervated FDB muscle fibers were first incubated with 10  $\mu\text{M}$  Ru360 for 30 min before receiving the field stimulation. Immediately, following the field stimulation (still in the presence of 10  $\mu\text{M}$  Ru360), the denervated FDB fibers were loaded with MitoSOX Red for evaluation of mitochondrial superoxide level. As shown in Fig. 7a4 and b, in the presence of Ru360, the field stimulation no longer reversed the elevated mitochondrial superoxide level in the denervated muscle fibers ( $15.15 \pm 5.16$ ,  $n = 5$ ,  $p < 0.05$  compared to the denervated fibers without Ru360), suggesting that the transient mitochondrial  $\text{Ca}^{2+}$  uptake is likely responsible

for suppressing the mitochondrial ROS production during a physiological  $\text{Ca}^{2+}$  release transient. We also conducted a control experiment to test if Ru360 has a potential effect on mitochondrial ROS production. As demonstrated in Fig. 7a1 and a2, Ru360 has no significant influence on mitochondrial superoxide production level.

## Discussion

Previously published studies on how  $\text{Ca}^{2+}$  signaling regulate mitochondrial ROS production in skeletal muscle mainly focused on the effect of a steady state level of  $\text{Ca}^{2+}$  inside mitochondria [40]. Here, we provide the first evidence that the dynamic uptake of  $\text{Ca}^{2+}$  by mitochondria may also be a key player in maintaining the physiological function of mitochondria. We showed that the time course of free  $\text{Ca}^{2+}$  level inside mitochondria follows the time course of cytosolic  $\text{Ca}^{2+}$  transient and that physiological changes in mitochondrial  $\text{Ca}^{2+}$  levels could be essential for maintaining the functional integrity of mitochondria. Following denervation, there is no action potential initiated in muscle fibers, and therefore, no  $\text{Ca}^{2+}$  transients in the cytosol and mitochondria. Mitochondria respond to this condition with increased ROS production that is associated with mPTP opening. Restoring the physiological  $\text{Ca}^{2+}$  transients by electric stimulation reduced the mitochondrial ROS production and stopped the repetitive mPTP opening in the denervated muscle fibers.

Motor neuron innervation is critical for the growth and maintenance of muscle fibers. Denervation is known to cause muscle atrophy, manifested in age-dependent sarcopenia and other neurological diseases, such as amyotrophic lateral sclerosis (ALS). Studies by other

investigators have shown that denervation leads to compromised EC coupling machinery in skeletal muscle [41] and altered mitochondrial metabolic function [42, 43]. The increase in ROS generation is a common event in skeletal muscle mitochondria under a variety of pathological conditions associated with denervation-induced muscle atrophy [10]. Excessive ROS generation contributes to apoptotic or necrotic cell death [22]. Biochemical assay has revealed that the ROS generation in muscle mitochondria was dramatically increased after several days of surgical sciatic nerve transection [10, 44]. It is believed that enhanced ROS generation is a common factor in the mechanism underlying denervation-induced muscle atrophy and the related downstream signaling pathways have been extensively studied [2, 11]. However, the initial signal that causes changes in the mitochondrial network and ROS production of skeletal muscle in response to denervation remains unknown. It is not clear whether the dynamic changes of the  $\text{Ca}^{2+}$  level in the cytosol and mitochondria are implicated in this process. Here, we provide evidence that physiological  $\text{Ca}^{2+}$  transient is required to maintain the integrity of mitochondrial function in the physiological condition. Absence of the physiological  $\text{Ca}^{2+}$  transients is likely a direct cause of enhanced mitochondrial ROS production that is associated with the repetitive opening of the mitochondrial mPTP.

Wang et al. developed a mitochondrial-targeted, circularly-permuted yellow fluorescent protein (mt-cpYFP) as an indicator of ROS production and energy metabolism of individual mitochondrion in live cells including skeletal muscle cells [25–27]. Their studies revealed that ROS is produced in transient waves at the level of individual mitochondria, a phenomenon known as the mitoflash [25]. Using the same transgene, we produced the mt-cpYFP transgenic mice in our laboratory and investigated the effect of denervation on mitochondrial function by monitoring the dynamic changes of mitoflash signals in mitochondria of live muscle fibers. Twenty-four hours following the sciatic nerve transection, denervated muscle fibers show an excessive increase in the mitoflash signal, specifically in the signal size (FAHM) that was four times larger than in control fibers. The data indicate that in a single muscle fiber, more mitochondria are activated to produce mitoflash signals in response to denervation. In addition, the Total Flash Area/Fiber Area of the mitoflash signal recorded during the 100-sequential-imaging time period was four times more than the controls, indicating a higher frequency of individual mitochondria to produce mitoflash activity.

In both skeletal and cardiac muscle cells, mitochondria form a structural and functional network [30, 45, 46]. Imaging of mitoflash signal of skeletal muscle in mt-cpYFP mice has also revealed functional mitochondrial network [27]. In the current study, the dramatic increase

in the size of the mitoflash signal (FAHM) could indicate that the mitochondrial network is physically more connected following denervation. However, this is unlikely, as a study by Romanello et al. has reported that denervation promotes mitochondrial fission activity, which should reduce the physical connection between mitochondria [47]. Our previous study has also identified a reduced mitochondrial network with enhanced fission activity in skeletal muscle of an ALS mouse model (G93A), in which skeletal muscle experiences denervation during ALS progression [30]. As identified in cardiac myocytes, the release of ROS from a subset of mitochondria can trigger ROS release from the adjacent mitochondria [48–50]. The dramatically enhanced size of mitoflash signal in skeletal muscle is likely an indication of the ROS-induced ROS release in mitochondria that is augmented by denervation. Other kinetic parameters such as the signal amplitude and FDHM stay the same, indicating that mitoflash kinetics was not affected by a short period (24 h) of denervation.

While mitochondria take up  $\text{Ca}^{2+}$  during skeletal muscle contraction [19, 20, 51], the mitochondrial  $\text{Ca}^{2+}$  uptake seems to be a double-edged sword for the fate of cells [22, 40]. Under normal conditions, mitochondrial  $\text{Ca}^{2+}$  uptake is a physiological stimulus for ATP synthesis [21, 52, 53]. The elevated mitochondrial  $\text{Ca}^{2+}$  level leads to a coordinated upregulation of oxidative phosphorylation machinery, resulting in higher mitochondrial ATP output to meet the energy demanding of the cells [54, 55]. This is required to meet the increased contractile force during muscle contraction. In addition, the mouse model (MCU<sup>-/-</sup>) with global knockout of mitochondrial calcium uniporter (MCU) showed a smaller body size and impaired skeletal muscle performance along with absence of mitochondrial  $\text{Ca}^{2+}$  uptake in isolated skeletal muscle mitochondria, indicating that mitochondrial  $\text{Ca}^{2+}$  uptake plays an important role in skeletal muscle development and performance [56]. However,  $\text{Ca}^{2+}$  overload in mitochondria is also a pathological stimulus of ROS generation [22]. It has been shown that prolonged skeletal muscle inactivity (such as muscle disuse) leads to an increased resting cytosolic free  $\text{Ca}^{2+}$  level, that in turn overloads mitochondria to stimulate the ROS production [23, 24]. While previous published studies on how  $\text{Ca}^{2+}$  signaling regulate mitochondrial ROS production in skeletal muscle mainly focused on the effect of a steady state level of  $\text{Ca}^{2+}$  inside mitochondria, it is not known whether the dynamic  $\text{Ca}^{2+}$  uptake by mitochondria has a role in maintaining the mitochondrial functional integrity. Recording of the mitoflash signal in a skeletal muscle fiber following a short period of denervation allowed us to discover the early response of mitochondria to the absence of physiological cytosolic  $\text{Ca}^{2+}$  transients, which limits mitochondrial

$\text{Ca}^{2+}$  uptake and leads to an excessive increase in mitochondrial ROS production. Our result is in line with the study by Csordas et al. [57], in which they found that destruction of the ER-mitochondria linkage causes the specific loss of the  $\text{IP}_3\text{R}$ -mediated  $\text{Ca}^{2+}$  transfer to mitochondria that stimulates oxidative metabolism in a cultured mammalian cell line [57]. Most importantly, we demonstrated that the early increase of mitochondrial ROS production was immediately diminished by restoring a train of physiological intracellular  $\text{Ca}^{2+}$  transients in denervated muscle fibers and that the transient mitochondrial  $\text{Ca}^{2+}$  uptake could be a key regulator of mitochondrial mPTP activity. Interestingly, recent studies from other research groups also provided evidence of MCU-dependent mitochondrial  $\text{Ca}^{2+}$  uptake in protecting denervation-induced skeletal muscle atrophy by using virus-mediated overexpression of MCU [58, 59]. While it is very well known that  $\text{Ca}^{2+}$  overload into mitochondria leads to mPTP opening and ROS production, one of the major findings in the present study is that the denervation-induced ROS elevation could be reduced by electrical stimulation, indicating an unexpected role of the  $\text{Ca}^{2+}$  uptake into mitochondria for control of ROS production. While a consistently elevated intracellular  $\text{Ca}^{2+}$  level leads to the  $\text{Ca}^{2+}$  overload in mitochondria and mPTP opening, the absence of physiological  $\text{Ca}^{2+}$  transients following denervation, which leads to the absence of the dynamic  $\text{Ca}^{2+}$  uptake into mitochondria, also triggers mPTP opening and initiates mitochondrial dysfunction. We speculate that there may be a biphasic dependence of mPTP on  $\text{Ca}^{2+}$  level or direct response to SR  $\text{Ca}^{2+}$  release. The molecular composition of mPTP is still incompletely understood. It is unclear what are the molecular mechanisms underlying the different responses of mitochondria to a consistently elevated intracellular  $\text{Ca}^{2+}$  level and to the absence of physiological  $\text{Ca}^{2+}$  transients following denervation. Future studies are needed to further understand the molecular mechanism underlying the initial response of mitochondria to denervation in skeletal muscle.

While denervation eliminates neuromuscular transmission and myoplasmic  $\text{Ca}^{2+}$  transients, other muscle adaptations and changes can occur during the first 24 h after denervation. One possibility is that mitochondrial and/or cellular ROS detoxification mechanisms (e.g., SOD, GSH reductase, catalase, and thioredoxin) may be reduced after denervation, and thus, allow for aberrant cell-wide propagation of otherwise spatially restricted mitochondrial ROS-related events. If bursts of ROS-related mitoflash activity are initiated by low-level increases in ROS, then a breakdown of cellular ROS detoxification mechanisms following denervation could also have a contribution to the observed increase in cell-wide waves of ROS-induced ROS release. Thus, changes to denervated fibers in addition to the loss of cytoplasmic

$\text{Ca}^{2+}$  transients and mitochondrial  $\text{Ca}^{2+}$  uptake are needed to explain the observed enhancement in mitoflash activity. More studies are needed to further understand the molecular mechanism for early response of skeletal muscle to denervation.

One concern about our result is the possibility that the drastic reduction of the mitoflash signal in the denervated muscle fibers following the tetanic field stimulation is due to the cell damage caused by the tetanic field stimulation. We were aware of the study of mitoflash signal on normal skeletal muscle by Wei and colleagues who reported that the mitoflash frequency was significantly increased following a 2-s tetanic stimulation and markedly decreased following prolonged 20-s tetanic stimulation [37]. As a result, the rationale for our experiment design is to avoid the 2-sec tetanic stimulation that already showed promoting mitoflash activity. We also decided not to use 20-s stimulation, as we do not know if the 20-s tetanic stimulation could cause artificial responses in our study. Instead, we applied a tetanic stimulation with much shorter duration (350 ms). Thus, the reduction in mitoflash signal observed in the denervated muscle fibers following such a brief electrical stimulation is unlikely due to the physical damage caused by the field stimulation. Interestingly, this brief stimulation also suppressed the mitoflash activity in the sham muscle. Our data together with the previous study by Wei et al., suggest that the response of mitochondria to tetanic stimulation is dynamic, and the underlying molecular mechanisms may be different between the 350-ms stimulation and 2-s stimulation. It is not a surprise to see that a sevenfold longer electric stimulation (2 s) enhances the mitoflash activity, as it likely promotes more mitochondrial  $\text{Ca}^{2+}$  uptake, which is known to promote the function of the respiratory chain reaction.

We previously demonstrated that mitochondria in skeletal muscle take up  $\text{Ca}^{2+}$  following a brief electric stimulation [20]. Here, we showed that during prolonged membrane depolarization, mitochondrial  $\text{Ca}^{2+}$  transient also follows a similar time course as the cytosolic  $\text{Ca}^{2+}$  transient in skeletal muscle fibers. Our results support the hypothesis that the dynamic levels of  $\text{Ca}^{2+}$  inside mitochondria follow the time course of the cytosolic  $\text{Ca}^{2+}$  transients initiated by motor neuron activation in the physiological condition and that the dynamic change in mitochondrial  $\text{Ca}^{2+}$  level could serve as a sensor to decode the nerve innervation. While  $\text{Ca}^{2+}$  overload in mitochondria triggers more ROS production [22], our results indicate that absence of the physiological mitochondrial  $\text{Ca}^{2+}$  uptake also play a role for maintaining the integrity of normal mitochondrial function.

The coupling of mitoflash and mPTP opening has been well characterized in both cardiac and skeletal muscle [27, 35]. It has been shown that mt-cpYFP

fluorescence is transiently increased when the mitochondrial membrane potential (measured by TMRE) is depolarized during a dual recording, indicating a dynamic coupling of the mitoflash event and the mPTP opening. Several lines of evidence have suggested a strong connection between CypD-related mPTP opening and the mitoflash signal in cardiac muscle but not in normal skeletal muscle. Indeed, manipulation of mPTP had a major impact on the mitoflash signal in cardiac myocytes. For example, activators of mPTP, like atractyloside, increased the mitoflash frequency in cardiac myocytes [26] but not in skeletal muscle fibers [36]. In contrast, CypD inhibitors such as cyclosporine A (CsA) caused a reduction in the mitoflash amplitude and kinetics in cardiac myocytes [26]. However, CsA did not appear to affect the mitoflash signal in skeletal muscle fibers under normal physiological conditions [36, 37], indicating that the mitoflash signal in normal skeletal muscle may not be related to the activity of CypD at physiological conditions. Remarkably, we demonstrated that in the case of denervation, the enhanced mitoflash signal might directly associated with the CypD-related opening of mPTP in skeletal muscle fibers. Incubation with 1  $\mu$ M CsA for 30 min significantly reduced the Total Flash Area/Fiber Area, FAHM, and the amplitude of the mitoflash in denervated muscle fibers. CsA inhibits mPTP opening by binding to Cyclophilin D (CypD) [60]. Thus, the apparent relationship between mPTP and the mitoflash signal seems to be related on CypD in the denervated muscle. It has been shown that knocking down CypD with siRNA, a major component related to mPTP, significantly reduced mitoflash frequency in cardiac myocytes [26, 61]. The opposite occurred upon CypD overexpression [61]. Based on a biochemical study, Csukly K et al. has shown that following 3 weeks of denervation, the isolated mitochondria from denervated muscle have enhanced vulnerability to  $\text{Ca}^{2+}$ -induced mPTP opening, and this  $\text{Ca}^{2+}$ -induced mPTP opening can be blocked by the application of CsA. In addition, the relative level of CypD is increased in mitochondrial fraction of the denervated skeletal muscle, indicating a CypD-related mPTP opening in denervated muscle [42]. In line with this discovery, we found that 24-h denervation led to an increase in the ratio of CypD-mito/CypD-cyto. The increased ratio of CypD-mito/CypD-cyto could reflect increased degradation of the cytosolic CypD, increased stability of mitochondrial CypD, or increased translocation of CypD from the cytosol to mitochondria. Nevertheless, the increased ratio indicates a relative change of CypD in mitochondria fraction. This result together with the pharmacological study of CsA suggests that CypD is likely involved in regulating mPTP activity and mitochondrial ROS production in skeletal muscle following

1 day of denervation. Although it is very well established that CsA inhibits mPTP by binding to CypD and has been extensively used as an investigative tool for mPTP research, it is also known that CsA inhibits calcineurin, a calcium dependent dephosphorylation enzyme [60, 62]. Studies by Cereghetti et al. and Cribbs and Strack demonstrate the role of calcineurin in dephosphorylation of Drp1, which promotes mitochondrial fission [63, 64]. It has been found that CsA promotes mitochondrial fusion through inhibition of calcineurin [63, 65]. Thus, it is possible that the reduced mitoflash activity in the presence of CsA may also partially due to the enhanced mitochondrial fusion, which indirectly affects the mitochondrial ROS production. Nevertheless, our result with relatively enhanced mitochondrial CypD level and the published study showing an enhanced CypD expression level in skeletal muscle with prolonged denervation suggest a potential involvement of the CypD-related mPTP opening in skeletal muscle in response to denervation. The CypD-related mPTP opening is likely an early event in skeletal muscle mitochondria in response to denervation. Most importantly, for the first time, our data demonstrated that the physiological  $\text{Ca}^{2+}$  transients and the following mitochondrial  $\text{Ca}^{2+}$  uptake play a key role in maintaining the functional integrity of mitochondria through a potential mechanism by regulating the mPTP-related mitochondrial ROS production.

Although mt-cpYFP has been characterized and used as a biomarker of mitochondrial ROS generation [26, 36, 37], there are concerns about the specificity of the mitoflash signal. It has been suggested that mitoflash may also report ATP [66] or pH changes inside mitochondrial matrix [34, 67]. Nevertheless, the mitoflash signal may reflect the status of the ROS-related metabolic function of mitochondria, and cpYFP likely can report both ROS and pH signal of mitochondria, and is thus a robust biosensor for mitochondrial function [68, 69]. However, the portion of ROS vs pH signal reported by the mitoflash signal could be context-dependent [35]. Such detailed quantification will require additional measurement, which is not the focus of the current study. A recent study by Ding et al. indicates that mitoflash represents a dynamic signal of mitochondrial ROS production and energy metabolism [25]. In our current study, mitoflash signal served as a unique biosensor that allowed us to dissect the early response of mitochondria to denervation and to identify the role of physiological  $\text{Ca}^{2+}$  transients in maintaining the functional integrity of mitochondria in skeletal muscle. Due to the ongoing debate of mt-cpYFP sensitivity on ROS and pH [34], we used MitoSOX Red, a separate fluorescent indicator for mitochondrial superoxide detection, to further evaluate the response of denervated muscle fibers to electrical stimulation. Although MitoSOX Red is not able to detect the dynamic changes of mitochondrial ROS

production, its fluorescence intensity can report the basal level of mitochondrial superoxide production. Our MitoSOX Red data confirmed that mitochondrial ROS production was enhanced following 24 h of denervation and that electrical stimulation could reverse mitochondrial ROS production to basal level.

## Conclusions

In summary, we have taken advantage of the transgenic mt-cpYFP mice that allowed us to evaluate the early dynamic response of skeletal muscle to denervation at the mitochondrial level of live muscle fibers. For the first time, our study reveals that physiological  $\text{Ca}^{2+}$  transient is important for maintaining the normal mitochondrial metabolic function by regulating the mPTP-associated mitochondrial ROS generation. Combining voltage-clamp technique and live skeletal muscle cell imaging study, we showed that the  $\text{Ca}^{2+}$  level inside mitochondria of skeletal muscle is synchronized with the dynamic change of cytosolic  $\text{Ca}^{2+}$  level under physiological condition. In the case of denervation, there are no  $\text{Ca}^{2+}$  transients initiated in the cytosol and thus no dynamic alterations in mitochondrial  $\text{Ca}^{2+}$  level. Our study suggests that the dynamic change of  $\text{Ca}^{2+}$  level inside mitochondria regulates the mitochondrial ROS generation as a response to the cytosolic  $\text{Ca}^{2+}$  transient in the physiological condition. Additionally, mitochondria in denervated muscle fibers could sense the absence of the physiological  $\text{Ca}^{2+}$  transients and respond with enhanced ROS generation that could initiate downstream signaling toward mitochondrial dysfunction. Future studies should focus on the detailed molecular basis underlying the mitochondrial response to the absence of physiological  $\text{Ca}^{2+}$  transients.

## Additional files

**Additional file 1: Figure S1.** Live cell imaging shows the mitochondrial targeting of mt-cpYFP in skeletal muscle of the transgenic mice (cpYFP). mt-cpYFP targeted well to mitochondria in skeletal muscle of the transgenic mice cpYFP. The representative images of FDB muscle fibers enzyme-isolated from the transgenic mouse cpYFP were incubated with 50 nM TMRE for 10 min. A. Muscle fibers expressing mt-cpYFP. B. TMRE marked mitochondria of the same muscle fibers in A. C. Overlay of A and B indicates the targeting of mt-cpYFP to mitochondria. (PDF 304 kb)

**Additional file 2: movie 1.** Mitoflash recording of a denervated muscle fiber; 012Den4231\_movie1. (AVI 1458 kb)

**Additional file 3: movie 2.** Mitoflash recording of a fiber with the sham procedure; 009CL4413\_movie2. (AVI 1182 kb)

**Additional file 4: movie 3.** Mitoflash recording of a denervated fiber in the presence of CsA; 004CsA72513\_movie3. (AVI 976 kb)

**Additional file 5: Figure S2.** The pure mitochondria and cytosol fractions do not show contamination from each other. The COX-IV antibody only detects bands in pure mitochondrial fraction, not in cytosol fraction, while the GAPDH antibody only detects bands in the cytosol fraction. (PDF 174 kb)

**Additional file 6: Movie 4.** Mitoflash recording of a denervated muscle fiber before electric stimulation; 005BeforeDenStim050614\_movie4. (AVI 1634 kb)

**Additional file 7: Movie 5.** Mitoflash recording of a denervated muscle fiber 10 s after the electric stimulation; 005aDenStim050614\_movie5. (AVI 1334 kb)

## Abbreviations

ALS: Amyotrophic lateral sclerosis; CsA: Cyclosporine A; CypD: Cyclophilin D; E-C coupling: Excitation-contraction coupling; FAHM: Full amplitude of half maximum; FDB: Flexor digitorum brevis; FDHM: Full duration of half maximum; mPTP: Mitochondrial transition pore; mt-cpYFP: Mitochondrial targeted biosensor; ROS: Reactive oxygen species; SR: Sarcoplasmic reticulum

## Acknowledgements

We appreciate Mr. Frank Yi for editing this manuscript.

## Funding

This work was fully supported by Muscular Dystrophy Association Grant MDA-4351 and NIAMS/National Institutes of Health Grant R01 AR057404 to JZ and partially supported by R01-AG028614 to JM. CK was a recipient of a postdoctoral fellowship from NIH/NHLBI T32 training grant HL 07692-(21-25). LZ was a recipient of a scholarship from Zunyi Medical University. JZ laboratory is also supported by Victor E. Speas Foundation and McCown Gordon Gala Research Gift.

## Availability of data and materials

All data generated or analyzed during this study are included in this published article.

## Authors' contributions

JZ designed and supervised the study. JM and JY participated the experimental design of the study. JZ, JM, CK, and JY wrote the manuscript. CK, JY, YX, KD, JZ, XL, and CM performed the experiments. CK, KD, YX, JY, JM, and JZ analyzed the data. KL and JX assisted running the image-process software. HC participated in the scientific discussion on this study. All authors read and approved the final manuscript.

## Competing interests

The authors declare that they have no competing interests.

## Consent for publication

Not applicable.

## Ethics approval

All animal experiments were performed according to the procedures approved by Institutional Animal Care and Use Committee of Rush University Medical Center, University of Missouri at Kansas City, and Kansas City University.

## Publisher's Note

Springer Nature remains neutral with regard to jurisdictional claims in published maps and institutional affiliations.

## Author details

<sup>1</sup>Rush University School of Medicine, Chicago, IL, USA. <sup>2</sup>Kansas City University of Medicine and Bioscience, 1750 Independence Ave, Kansas City, MO 64106, USA. <sup>3</sup>Institute of Molecular Medicine, Peking University, Beijing, China. <sup>4</sup>Wexner Medical Center, The Ohio State University, 460 West 12th Avenue, Columbus, OH, USA.

Received: 8 December 2016 Accepted: 8 March 2017

Published online: 10 April 2017

## References

1. Neel BA, Lin Y, Pessin JE. Skeletal muscle autophagy: a new metabolic regulator. *Trends Endocrinol Metab.* 2013;24:635–43.
2. Sandr M. Signaling in muscle atrophy and hypertrophy. *Physiology (Bethesda).* 2008;23:160–70.



3. Bodine SC, Latres E, Baumhueter S, Lai VK, Nunez L, Clarke BA, Poueymirou WT, Panaro FJ, Na E, Dharmarajan K, Pan ZQ, Valenzuela DM, DeChiara TM, Stitt TN, Yancopoulos GD, Glass DJ. Identification of ubiquitin ligases required for skeletal muscle atrophy. *Science*. 2001;294:1704–8.
4. Clarke BA, Drujan D, Willis MS, Murphy LO, Corpina RA, Burova E, Rakhilin SV, Stitt TN, Patterson C, Latres E, Glass DJ. The E3 Ligase MuRF1 degrades myosin heavy chain protein in dexamethasone-treated skeletal muscle. *Cell Metab*. 2007;6:376–85.
5. Furuno K, Goodman MN, Goldberg AL. Role of different proteolytic systems in the degradation of muscle proteins during denervation atrophy. *J Biol Chem*. 1990;265:8550–7.
6. Gomes MD, Lecker SH, Jagoe RT, Navon A, Goldberg AL. Atrogin-1, a muscle-specific F-box protein highly expressed during muscle atrophy. *Proc Natl Acad Sci U S A*. 2001;98:14440–5.
7. Sandri M, Sandri C, Gilbert A, Skurk C, Calabria E, Picard A, Walsh K, Schiaffino S, Lecker SH, Goldberg AL. Foxo transcription factors induce the atrophy-related ubiquitin ligase atrogin-1 and cause skeletal muscle atrophy. *Cell*. 2004;117:399–412.
8. Stitt TN, Drujan D, Clarke BA, Panaro F, Timofeyeva Y, Kline WO, Gonzalez M, Yancopoulos GD, Glass DJ. The IGF-1/PI3K/Akt pathway prevents expression of muscle atrophy-induced ubiquitin ligases by inhibiting FOXO transcription factors. *Mol Cell*. 2004;14:395–403.
9. Eisenberg BR. Quantitative Ultrastructure of Mammalian Skeletal Muscle. In Peachey LD, Adrian RH and Geiger SR (Ed.). Baltimore: American Physiological Society. *Skeletal Muscle*. 1983;10:73–112.
10. Muller FL, Song W, Jang YC, Liu Y, Sabia M, Richardson A, Van Remmen H. Denervation-induced skeletal muscle atrophy is associated with increased mitochondrial ROS production. *Am J Physiol Regul Integr Comp Physiol*. 2007;293:R1159–68.
11. Powers SK, Wiggs MP, Duarte JA, Zergeroglu AM, Demirel HA. Mitochondrial signaling contributes to disuse muscle atrophy. *Am J Physiol Endocrinol Metab*. 2012;303:E31–9.
12. Payne AM, Jimenez-Moreno R, Wang ZM, Messi ML, Delbono O. Role of  $Ca^{2+}$ , membrane excitability, and  $Ca^{2+}$  stores in failing muscle contraction with aging. *Exp Gerontol*. 2009;44:261–73.
13. Weisleder N, Brotto M, Komazaki S, Pan Z, Zhao X, Nosek T, Parness J, Takeshima H, Ma J. Muscle aging is associated with compromised  $Ca^{2+}$  spark signaling and segregated intracellular  $Ca^{2+}$  release. *J Cell Biol*. 2006;174:639–45.
14. De Backer F, Vandebrouck C, Gailly P, Gillis JM. Long-term study of  $Ca^{2+}$  homeostasis and of survival in collagenase-isolated muscle fibres from normal and mdx mice. *J Physiol*. 2002;542:855–65.
15. DiFranco M, Woods CE, Capote J, Vergara JL. Dystrophic skeletal muscle fibers display alterations at the level of calcium microdomains. *Proc Natl Acad Sci U S A*. 2008;105:14698–703.
16. Han R, Grounds MD, Bakker AJ. Measurement of sub-membrane  $[Ca^{2+}]_i$  in adult myofibers and cytosolic  $[Ca^{2+}]_i$  in myotubes from normal and mdx mice using the  $Ca^{2+}$  indicator FFP-18. *Cell Calcium*. 2006;40:299–307.
17. Wang X, Weisleder N, Collet C, Zhou J, Chu Y, Hirata Y, Zhao X, Pan Z, Brotto M, Cheng H, Ma J. Uncontrolled calcium sparks act as a dystrophic signal for mammalian skeletal muscle. *Nat Cell Biol*. 2005;7:525–30.
18. Szabadkai G, Duchen MR. Mitochondria: the hub of cellular  $Ca^{2+}$  signaling. *Physiology (Bethesda)*. 2008;23:84–94.
19. Zhou J, Yi J, Fu R, Liu E, Siddique T, Rios E, Deng HX. Hyperactive intracellular calcium signaling associated with localized mitochondrial defects in skeletal muscle of an animal model of amyotrophic lateral sclerosis. *J Biol Chem*. 2010;285:705–12.
20. Yi J, Ma C, Li Y, Weisleder N, Rios E, Ma J, Zhou J. Mitochondrial calcium uptake regulates rapid calcium transients in skeletal muscle during excitation-contraction (E-C) coupling. *J Biol Chem*. 2011;286:32436–43.
21. Kavanagh NI, Ainscow EK, Brand MD. Calcium regulation of oxidative phosphorylation in rat skeletal muscle mitochondria. *Biochim Biophys Acta*. 2000;1457:57–70.
22. Brookes PS, Yoon Y, Robotham JL, Anders MW, Sheu SS. Calcium, ATP, and ROS: a mitochondrial love-hate triangle. *Am J Physiol Cell Physiol*. 2004;287:C817–33.
23. Ingalls CP, Warren GL, Armstrong RB. Intracellular  $Ca^{2+}$  transients in mouse soleus muscle after hindlimb unloading and reloading. *J Appl Physiol*. 1999;87:386–90.
24. Tischler ME, Rosenberg S, Satarug S, Henriksen EJ, Kirby CR, Tome M, Chase P. Different mechanisms of increased proteolysis in atrophy induced by denervation or unweighting of rat soleus muscle. *Metabolism*. 1990;39:756–63.
25. Ding Y, Fang H, Shang W, Xiao Y, Sun T, Hou N, Pan L, Sun X, Ma Q, Zhou J, Wang X, Zhang X, Cheng H. Mitoflash altered by metabolic stress in insulin-resistant skeletal muscle. *J Mol Med*. 2015;93(10):1119–30.
26. Wang W, Fang H, Groom L, Cheng A, Zhang W, Liu J, Wang X, Li K, Han P, Zheng M, Yin J, Wang W, Mattson MP, Kao JP, Lakatta EG, Sheu SS, Ouyang K, Chen J, Dirksen RT, et al. Superoxide flashes in single mitochondria. *Cell*. 2008;134:279–90.
27. Fang H, Chen M, Ding Y, Shang W, Xu J, Zhang X, Zhang W, Li K, Xiao Y, Gao F, Shang S, Li JC, Tian XL, Wang SQ, Zhou J, Weisleder N, Ma J, Ouyang K, Chen J, et al. Imaging superoxide flash and metabolism-coupled mitochondrial permeability transition in living animals. *Cell Res*. 2011;21:1295–304.
28. Li K, Zhang W, Fang H, Xie W, Liu J, Zhang W, Wang X, Wang W, Tan W, Cheng H. Superoxide flashes reveal novel properties of mitochondrial reactive oxygen species excitability in cardiomyocytes. *Biophys J*. 2012;102:1011–21.
29. Manno C, Figueroa L, Fitts R, Rios E. Confocal imaging of transmembrane voltage by SEER of di-8-ANEPPS. *J Gen Physiol*. 2013;141:371–87.
30. Luo G, Yi J, Ma C, Xiao Y, Yi F, Yu T, Zhou J. Defective mitochondrial dynamics is an early event in skeletal muscle of an amyotrophic lateral sclerosis mouse model. *PLoS One*. 2013;8:e82112.
31. Pouvreau S, Royer L, Yi J, Brum G, Meissner G, Rios E, Zhou J.  $Ca^{2+}$  sparks operated by membrane depolarization require isoform 3 ryanodine receptor channels in skeletal muscle. *Proc Natl Acad Sci U S A*. 2007;104:5235–40.
32. Wong M, Gertz B, Chestnut BA, Martin LJ. Mitochondrial DNMT3A and DNA methylation in skeletal muscle and CNS of transgenic mouse models of ALS. *Front Cell Neurosci*. 2013;7:279.
33. Frezza C, Cipolat S, Scorrano L. Organelle isolation: functional mitochondria from mouse liver, muscle and cultured fibroblasts. *Nat Protoc*. 2007;2:287–95.
34. Schwarzlander M, Wagner S, Ermakova YG, Belousov V, Radi R, Beckman JS, Buettner GR, Demareux N, Duchen MR, Forman HJ, Fricker MD, Gems D, Halestrap AP, Halliwell B, Jakob U, Johnston IG, Jones NS, Logan DC, Morgan B, et al. The 'mitoflash' probe cpYFP does not respond to superoxide. *Nature*. 2014;514:E12–4.
35. Wang W, Zhang H, Cheng H. Mitochondrial flashes: From indicator characterization to in vivo imaging. *Methods*. 2016;109:12–20.
36. Pouvreau S. Superoxide flashes in mouse skeletal muscle are produced by discrete arrays of active mitochondria operating coherently. *PLoS One*. 2010;5:e13035.
37. Wei L, Salahura G, Boncompagni S, Kasischke KA, Protasi F, Sheu SS, Dirksen RT. Mitochondrial superoxide flashes: metabolic biomarkers of skeletal muscle activity and disease. *FASEB J*. 2011;25:3068–78.
38. Matlib MA, Zhou Z, Knight S, Ahmed S, Choi KM, Krause-Bauer J, Phillips R, Altschuld R, Katsube Y, Sperelakis N, Bers DM. Oxygen-bridged dinuclear ruthenium amine complex specifically inhibits  $Ca^{2+}$  uptake into mitochondria in vitro and in situ in single cardiac myocytes. *J Biol Chem*. 1998;273:10223–31.
39. Nagai T, Yamada S, Tomimaga T, Ichikawa M, Miyawaki A. Expanded dynamic range of fluorescent indicators for  $Ca^{2+}$  by circularly permuted yellow fluorescent proteins. *Proc Natl Acad Sci U S A*. 2004;101:10554–9.
40. Zhou J, Dhakal K, Yi J. Mitochondrial  $Ca^{2+}$  uptake in skeletal muscle health and disease. *Sci China Life Sci*. 2016;59:770–6.
41. Delbono O, Chu A.  $Ca^{2+}$  release channels in rat denervated skeletal muscles. *Exp Physiol*. 1995;80:561–74.
42. Csukly K, Ascah A, Matas J, Gardiner PF, Fontaine E, Burelle Y. Muscle denervation promotes opening of the permeability transition pore and increases the expression of cyclophilin D. *J Physiol*. 2006;574:319–27.
43. Siu PM, Alway SE. Mitochondria-associated apoptotic signalling in denervated rat skeletal muscle. *J Physiol*. 2005;565:309–23.
44. Adhichetty PJ, O'Leary MF, Chabi B, Wicks KL, Hood DA. Effect of denervation on mitochondrially mediated apoptosis in skeletal muscle. *J Appl Physiol*. 2007;102:1143–51.
45. Eisner V, Lenaers G, Hajnoczky G. Mitochondrial fusion is frequent in skeletal muscle and supports excitation-contraction coupling. *J Cell Biol*. 2014;205:179–95.
46. Huang X, Sun L, Ji S, Zhao T, Zhang W, Xu J, Zhang J, Wang Y, Wang X, Franzini-Armstrong C, Zheng M, Cheng H. Kissing and nanotunneling mediate intermitochondrial communication in the heart. *Proc Natl Acad Sci U S A*. 2013;110:2846–51.
47. Romanello V, Guadagnin E, Gomes L, Roder I, Sandri C, Petersen Y, Milan G, Masiero E, Del Piccolo P, Foretz M, Scorrano L, Rudolf R, Sandri M. Mitochondrial fission and remodelling contributes to muscle atrophy. *EMBO J*. 2010;29:1774–85.

48. Aon MA, Cortassa S, O'Rourke B. Mitochondrial oscillations in physiology and pathophysiology. *Adv Exp Med Biol*. 2008;641:98–117.
49. Pacher P, Hajnoczky G. Propagation of the apoptotic signal by mitochondrial waves. *EMBO J*. 2001;20:4107–21.
50. Zorov DB, Juhaszova M, Sollott SJ. Mitochondrial reactive oxygen species (ROS) and ROS-induced ROS release. *Physiol Rev*. 2014;94:909–50.
51. Ainsbinder A, Boncompagni S, Protasi F, Dirksen RT. Role of Mitofusin-2 in mitochondrial localization and calcium uptake in skeletal muscle. *Cell Calcium*. 2015;57:14–24.
52. Hansford RG, Zorov D. Role of mitochondrial calcium transport in the control of substrate oxidation. *Mol Cell Biochem*. 1998;184:359–69.
53. McCormack JG, Denton RM. Mitochondrial  $\text{Ca}^{2+}$  transport and the role of intramitochondrial  $\text{Ca}^{2+}$  in the regulation of energy metabolism. *Dev Neurosci*. 1993;15:165–73.
54. Balaban RS. Cardiac energy metabolism homeostasis: role of cytosolic calcium. *J Mol Cell Cardiol*. 2002;34:1259–71.
55. Das AM, Harris DA. Intracellular calcium as a regulator of the mitochondrial ATP synthase in cultured cardiomyocytes. *Biochem Soc Trans*. 1990;18:554–5.
56. Pan X, Liu J, Nguyen T, Liu C, Sun J, Teng Y, Fergusson MM, Rovira II, Allen M, Springer DA, Aponte AM, Gucek M, Balaban RS, Murphy E, Finkel T. The physiological role of mitochondrial calcium revealed by mice lacking the mitochondrial calcium uniporter. *Nat Cell Biol*. 2013;15:1464–72.
57. Csordas G, Renken C, Varnai P, Walter L, Weaver D, Buttler KF, Balla T, Mannella CA, Hajnoczky G. Structural and functional features and significance of the physical linkage between ER and mitochondria. *J Cell Biol*. 2006;174:915–21.
58. Chemello F, Mammucari C, Gherardi G, Rizzuto R, Lanfranchi G, Cagnin S. Gene expression changes of single skeletal muscle fibers in response to modulation of the mitochondrial calcium uniporter (MCU). *Genomics Data*. 2015;5:64–7.
59. Mammucari C, Gherardi G, Zamparo I, Raffaello A, Boncompagni S, Chemello F, Cagnin S, Braga A, Zanin S, Pallafacchina G, Zentilin L, Sandri M, De Stefani D, Protasi F, Lanfranchi G, Rizzuto R. The mitochondrial calcium uniporter controls skeletal muscle trophism in vivo. *Cell Rep*. 2015;10:1269–79.
60. Hausenloy DJ, Boston-Griffiths EA, Yellon DM. Cyclosporin A and cardioprotection: from investigative tool to therapeutic agent. *Br J Pharmacol*. 2012;165:1235–45.
61. Ma Q, Fang H, Shang W, Liu L, Xu Z, Ye T, Wang X, Zheng M, Chen Q, Cheng H. Superoxide flashes: early mitochondrial signals for oxidative stress-induced apoptosis. *J Biol Chem*. 2011;286:27573–81.
62. Sileikyte J, Forte M. Shutting down the pore: the search for small molecule inhibitors of the mitochondrial permeability transition. *Biochim Biophys Acta*. 2016;1857:1197–202.
63. Cereghetti GM, Stangherlin A, Martins de Brito O, Chang CR, Blackstone C, Bernardi P, Scorrano L. Dephosphorylation by calcineurin regulates translocation of Drp1 to mitochondria. *Proc Natl Acad Sci U S A*. 2008;105:15803–8.
64. Cribbs JT, Strack S. Reversible phosphorylation of Drp1 by cyclic AMP-dependent protein kinase and calcineurin regulates mitochondrial fission and cell death. *EMBO Rep*. 2007;8:939–44.
65. Park J, Choi H, Kim B, Chae U, Lee DG, Lee SR, Lee S, Lee HS, Lee DS. Peroxiredoxin 5 (Prx5) decreases LPS-induced microglial activation through regulation of  $\text{Ca}^{2+}$ /Calcineurin-Drp1-dependent mitochondrial fission. *Free Radic Biol Med*. 2016;99:392–404.
66. Muller FL. A critical evaluation of cpYFP as a probe for superoxide. *Free Radic Biol Med*. 2009;47:1779–80.
67. Schwarzlander M, Logan DC, Fricker MD, Sweetlove LJ. The circularly permuted yellow fluorescent protein cpYFP that has been used as a superoxide probe is highly responsive to pH but not superoxide in mitochondria: implications for the existence of superoxide 'flashes'. *Biochem J*. 2011;437:381–7.
68. Wei-LaPierre L, Gong G, Gerstner BJ, Ducreux S, Yule DI, Pouvreau S, Wang X, Sheu SS, Cheng H, Dirksen RT, Wang W. Respective contribution of mitochondrial superoxide and pH to mitochondria-targeted circularly permuted yellow fluorescent protein (mt-cpYFP) flash activity. *J Biol Chem*. 2013;288:10567–77.
69. Zhang M, Sun T, Jian C, Lei L, Han P, Lv Q, Yang R, Zhou X, Xu J, Hu Y, Men Y, Huang Y, Zhang C, Zhu X, Wang X, Cheng H, Xiong JW. Remodeling of mitochondrial flashes in muscular development and dystrophy in zebrafish. *PLoS One*. 2015;10:e0132567.

Submit your next manuscript to BioMed Central and we will help you at every step:

- We accept pre-submission inquiries
- Our selector tool helps you to find the most relevant journal
- We provide round the clock customer support
- Convenient online submission
- Thorough peer review
- Inclusion in PubMed and all major indexing services
- Maximum visibility for your research

Submit your manuscript at  
[www.biomedcentral.com/submit](http://www.biomedcentral.com/submit)

